Miner Deposita (2015) 50:1007–1029
DOI 10.1007/s00126-015-0585-0

ARTICLE

Platinum-group minerals in the Limoeiro Ni–Cu–(PGE) sulfide deposit, Brazil: the effect of magmatic and upper amphibolite to granulite metamorphic processes on PGM formation

J. Mota-e-Silva[1,2] · H. M. Prichard[3] · C. F. Ferreira Filho[2] · P. C. Fisher[3] · I. McDonald[3]

Received: 19 February 2014 / Accepted: 10 March 2015 / Published online: 28 March 2015

Abstract The Limoeiro Ni–Cu–(platinum-group elements (PGE)) deposit is a recent discovery associated with an igneous tubular conduit system in northeastern Brazil. Representative ores from the deposit have been used for platinum-group minerals (PGM) identification and for PGE in base metal sulfides (BMS) quantification. Ninety-eighty percent of the PGM in the massive sulfide ores is homogeneous Pt–Ni–Bi-bearing merenskyite ($PdTe_2$) enclosed primarily by pyrrhotite, suggesting that it is formed by exsolution from monosulfide solid solution (MSS). Merenskyite gradually but systematically becomes poorer in Pt and Ni with increasing fractionation, which is interpreted to reflect a transition to a more evolved sulfide liquid that segregated in the eastern parts of the intrusion. In massive sulfide ores, merenskyite forms unusually large (up to 5000 μm^2) euhedral grains, commonly in contact with spherical silicate inclusions. BMS hosts 12–16 % of the Pd, with the remainder hosted by PGM, which is interpreted to indicate that merenskyite recrystallized from a PGE-bearing bismuthotelluride metamorphic melt formed during high-grade metamorphism. Sperrylite ($PtAs_2$) is the second most abundant PGM (18 % of PGM in disseminated ore) and in contrast to merenskyite occurs mainly as very small (median of 25 μm^2) inclusions in high-temperature silicates and oxides, interpreted to have crystallized at high temperatures directly from sulfide blebs that formed and were transported within the Limoeiro magma conduit.

Keywords Platinum-group-minerals · Merenskyite · Upper amphibolite to granulite facies metamorphism · Sperrylite · Ni–Cu–PGE sulfide deposit · Platinum-group elements

Editorial handling: C.M. Lesher and G. Beaudoin

Electronic supplementary material The online version of this article (doi:10.1007/s00126-015-0585-0) contains supplementary material, which is available to authorized users.

✉ J. Mota-e-Silva
jonasmotaesilva@gmail.com

[1] Votorantim Metals, Rua Luiz Benezato, 500, Jundiaí, SP 13212-161, Brazil

[2] Instituto de Geociências, Universidade de Brasilia, Brasília, DF 70900-970, Brazil

[3] School of Earth and Ocean Science, Cardiff University, Main Building, Park Place, Cardiff CF10 3AT, UK

Introduction

Magmatic nickel–copper–platinum-group element (Ni–Cu–platinum-group elements (PGE)) sulfide deposits form as a result of the segregation and concentration of droplets of sulfide liquid from a silicate mafic or ultramafic magma and the partitioning of chalcophile elements into this phase (Naldrett 2004). Platinum-group element-dominated deposits are more commonly associated with sulfide-poor (0.5–5 vol.%) orebodies such as those occuring in the Merensky Reef and Platreef in the Bushveld complex in the Republic of South Africa (Naldrett et al. 2008), the Great Dyke in Zimbabwe (Wilson et al. 2000), and the Stillwater complex in the USA (Godel and Barnes 2008). In contrast, the major Ni–Cu sulfide deposits are characterized by sulfide-rich (20–90 vol.%) rocks, such as in the Noril'sk-Talnakh deposits (Lightfoot et al. 1990) in Russia, Sudbury in Canada (Lightfoot and Farrow 2002), and Jinchuan in China (Li et al. 2004), and in these cases, PGE are by-products. However, these PGE by-products in Ni–Cu sulfide deposits can be crucial for the economic viability of smaller low-grade Ni–Cu–(PGE) sulfide

deposits, such as the Limoeiro Ni–Cu–(PGE) sulfide deposit in Brazil.

The Limoeiro Ni–Cu–(PGE) deposit is located in NE Brazil and hosts 35 Mt at 0.25 % Ni, 0.27 % Cu, 0.40 ppm Pd, and 0.16 ppm Pt (Votorantim Metals unpublished). It was discovered in 2009 and is located within a complex, concentrically zoned, tube-like (chonolithic) sub-horizontal orthopyroxenite-harzburgite intrusion, interpreted to have formed in the geological setting of a dynamic multi-pulse mafic magma conduit (Mota-e-Silva et al. 2013). The absolute age of this intrusion is not yet known, but regional geological constraints suggest that both the intrusion and host rocks belong to a terrain older than the Brasiliano/Pan-African orogenic cycle (650–500 Ma). During this orogeny, the intrusion and its country rock were metamorphosed to upper amphibolite to granulite facies with a temperature range of between 700 and 850 °C according to the CMASH system (Opx-in and Chl-out isograd). The ultramafic rocks are also affected by a later low-temperature hydrothermal alteration (Mota-e-Silva et al. 2013). Studies from other deposits worldwide have shown that during hydrothermal alteration and greenschist facies metamorphism, recrystallize to a different mineral assemblage, and Pd-bearing platinum-group minerals (PGM) can be mobilized from the base metal sulfides (BMS) into the surrounding silicates (Fuchs and Rose 1974; Dillon-Leitch et al. 1986; Prichard et al. 2001; Seabrook et al. 2004; Wang et al. 2008). However, the effects of upper amphibolite to granulite facies metamorphism on PGM and PGE mobility are poorly understood.

This study exhibits the role of both magmatic and high-grade metamorphic processes on the formation and distribution of the PGM. The combination of the use of scanning electron microscope (SEM) and laser-ablation inductively coupled-plasma mass spectrometry (LA-ICP-MS) analyses enables us to examine the behavior of the PGE during the geological history of these ores, whether hosted by BMS or in discrete PGM grains. These results have the potential to improve ore processing in Limoeiro deposit, as well as to enhance the overall understanding of PGE and PGM in magmatic and metamorphic systems, especially during upper amphibolite to granulite facies metamorphism.

Geological setting

The Limoeiro Ni–Cu–(PGE) sulfide deposit

The Limoeiro Ni–Cu–(PGE) sulfide deposit is located in northeastern Brazil, in a high-grade mobile belt belonging to the Brasiliano orogenic cycle (650–500 Ma) known as the Borborema province (Almeida et al. 1981; Brito Neves et al. 2000; Santos et al. 2010) (Fig. 1). This intrusion has a chonolithic (tubular) form that potentially represents a magma conduit hosted within high-grade paragneiss and schist (Fig. 2). The conduit consists of two main distinct sequences of ultramafic rocks (upper and lower sequences), each consisting of a core of harzburgite (olivine-orthopyroxene± chromite cumulates) enveloped by orthopyroxenite (orthopyroxene-olivine±chromite cumulates), with an irregular and discontinuous outer shell of amphibolite (Fig. 3). A granoblastic texture consisting of equigranular medium-grained amphibole crystals with polygonal contacts is evidence of the metamorphic origin of the amphibolite rim. The ultramafic sequences, otherwise characterized by a similar composition and structure, have distinctly different S contents resulting from the presence of disseminated Ni–Cu sulfide mineralization only in the Upper Sequence. These sequences are believed to have been formed from the input of two major pulses of magma with similar compositions (Mota-e-Silva et al. 2013) but different sulfide saturation histories. Geological evidence and the variation of whole rock Ni/Cu and Cu/Pd ratios along the conduit (Mota-e-Silva and Ferreira Filho unpublished) indicate that the direction of the magma flux at the time that the Limoeiro intrusion formed was from the west to the east. For these reasons the intrusion appears to record a more primitive signature in the western ores and a more fractionated signature in the eastern ores.

The complex is metamorphosed and partly deformed. Peak metamorphic paragenesis for the ultramafic intrusion and country rocks indicate an upper amphibolite to granulite facies metamorphism represented by a metamorphic assemblage of anthophyllite, hornblende, phlogopite, chlorite, Al–Fe–Mg–Cr spinel coexisting with deformed and partially recrystallized relicts of larger orthopyroxene and olivine crystals that are occasionally surrounded by fine-grained polygonal aggregates (produced by metamorphic re-crystallization to sub-grains). The ultramafic rocks are also affected by a later low-temperature hydrothermal alteration, which is characterized by formation of antigorite with magnetite, talc, chlorite, and calcite (Mota-e-Silva et al. 2013). Deformed rocks, eventually transformed into phlogopitite in extreme cases, and tectonically remobilized sulfide stringers represent the products of tectonism and deformation throughout the complex. Such deformation is confined to shear zones and some parts of the outer contact of the intrusion with its country rocks.

On a broad scale, the mineralization still preserves its primary magmatic geometry, consisting of thick (up to 150 m) and elongated (up to 1 km) bodies of disseminated sulfides (2–10 vol.%; Fig. 4a) broadly concordant with the chonolithic structure. Massive ore (Fig. 4b) occurs just in the Retiro and Piçarra areas (Fig. 2) and represents about 3 vol.% of the Limoeiro deposit (Mota-e-Silva et al. 2013). Locally, tectonically mobilized sulfide stringers form narrower massive sulfide veins (Fig. 4c).

From west to east, the Limoeiro intrusion hosts ores in four areas: Parnazo, Retiro, Piçarra, and Bofe. The Retiro and

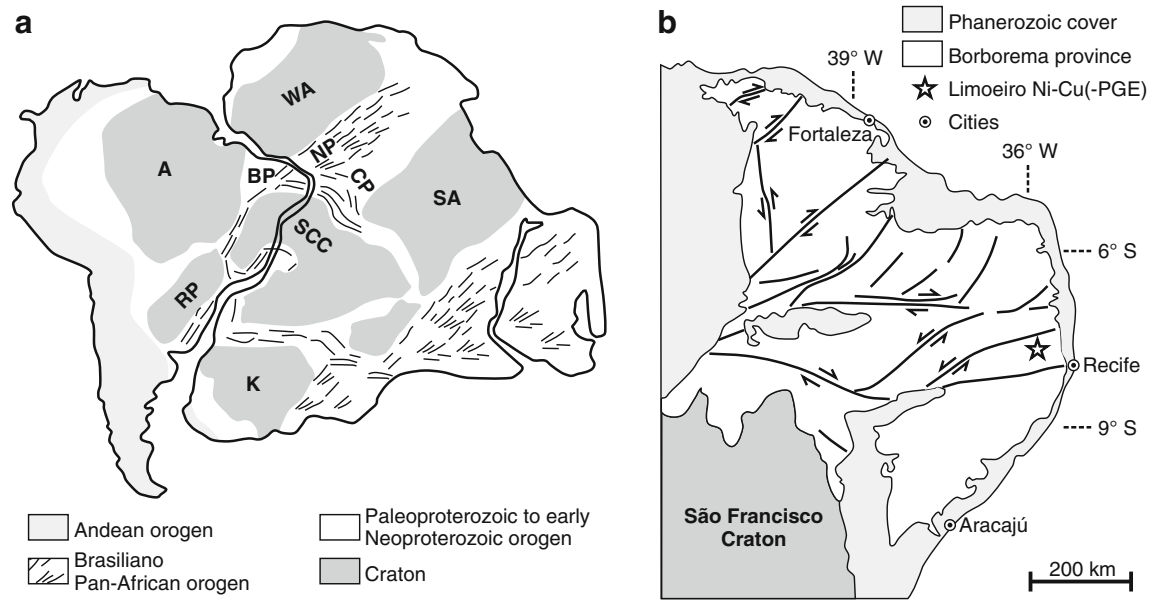

Fig. 1 **a** Pre-rift reconstruction of western Gondwana showing the main cratons and Brasiliano/Pan-African provinces (modified from Neves and Alcantara 2010). Abbreviations: *A* Amazonia, *BP* Borborema, *CP* Cameroon, *NP* Nigeria, *K* Kalahari, *RP* Rio de La Plata, *SA* Sahara Metacraton, *SCC* São Francisco/Congo, *WA* West Africa. **b** Map showing the position of Limoeiro Ni–Cu–(PGE) sulfide deposit in the Borborema province (modified from Mota-e-Silva et al. 2013)

Piçarra areas are the most extensively drilled, as they contain the only known economic mineralization in the Limoeiro intrusion (Fig. 2). The Retiro area has a more continuous, less faulted and less deformed structure, compared with the Piçarra area in which the distinction between igneous stratigraphic boundaries are not so well defined. Recent drilling reveals that the upper sequence is not the topmost sequence. It is located below a low-Cr sequence (Figs. 3 and 4), which is formed of the same rocks as the upper and lower sequences. The low-Cr sequence rocks have 150 to 850 ppm of Cr, whereas the upper and lower sequences range between 1120 and 2310 ppm Cr. Furthermore, between the upper and lower sequences has been identified a narrower but continuous transition zone layer (Figs. 5 and 6), that is generally sulfide-bearing. A better description and understanding of the significance of the low-Cr sequence and this transition zone is not the focus of this study.

Sampling and analytical methods

Fifteen half-drill cores of PGM mineralization were studied. These included the disseminated sulfide ore hosted in three different rock types (amphibolite, orthopyroxenite, and harzburgite) and also massive sulfide, in both primary and remobilized ores, from different parts of the chonolith.

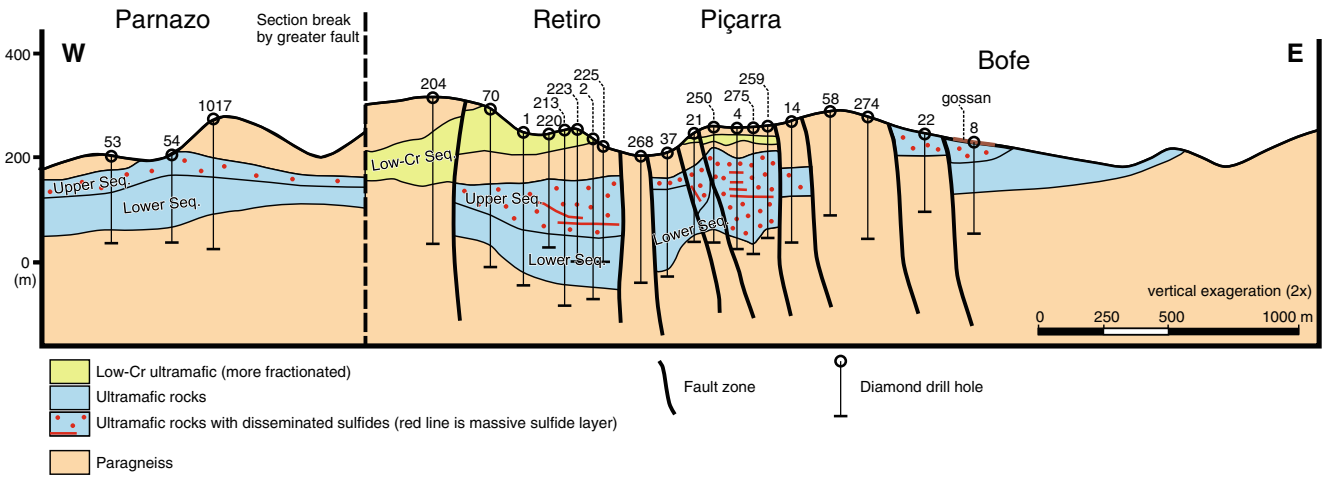

Fig. 2 Representative longitudinal section along the chonolithic structure. Note that the Upper sequence is the only sulfide-bearing unit in the Parnazo and Retiro targets. However, this feature is not clear in the very tectonically disrupted Piçarra target to the east. The density of *red circles* is proportional to sulfide abundance

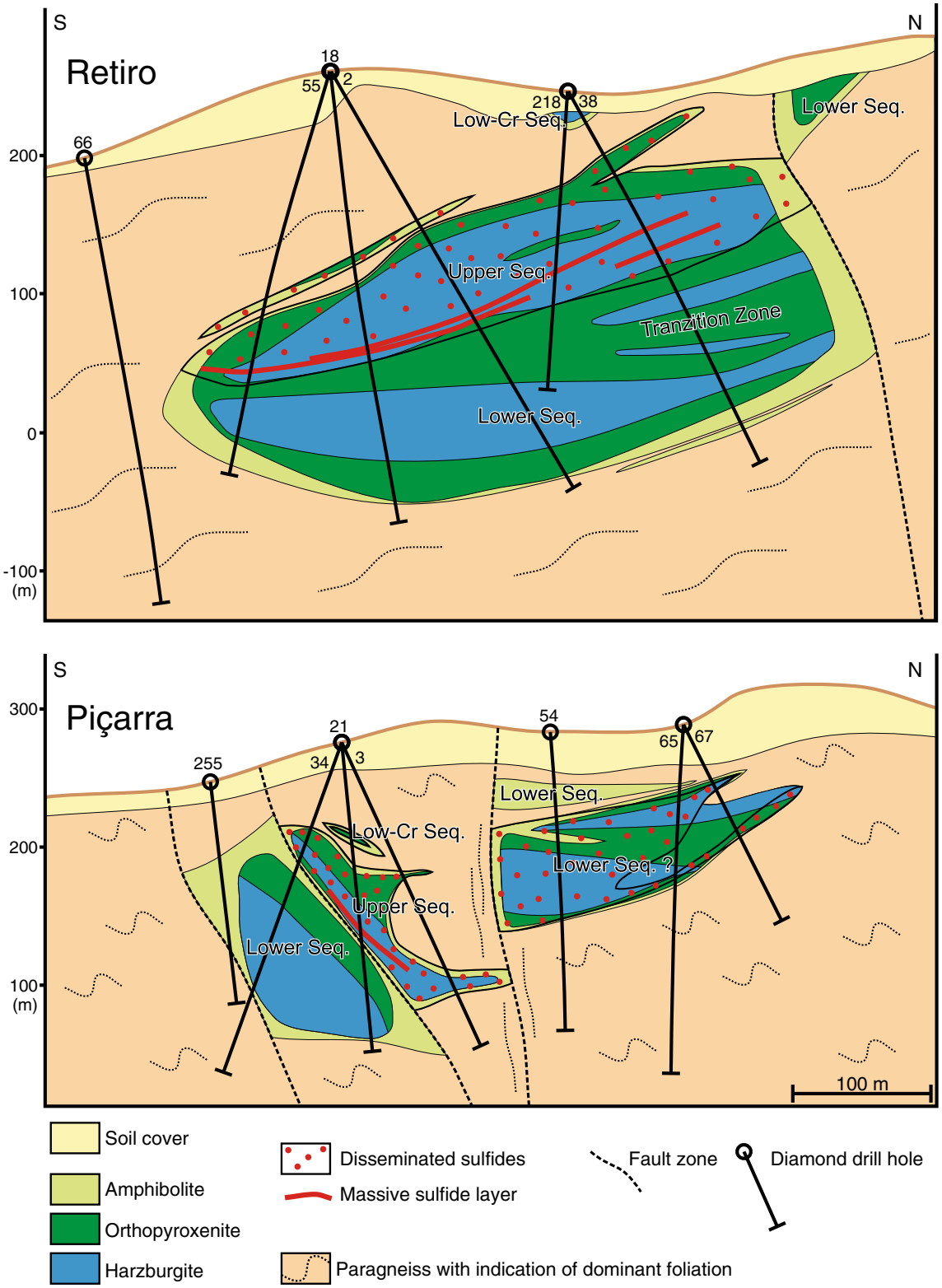

Fig. 3 Representative cross-sections of the two main drilling targets in the Limoeiro Ni–Cu–(PGE) sulfide deposit

Samples were analyzed from the western Retiro area, the most primitive part of the intrusion to be sampled, and from the eastern Piçarra area, which consists of more fractionated sulfides. PGM were identified using a four-quadrant back-scattered electron detector (4QBSD) on a Zeiss NTS S360 SEM at Cardiff University. The samples were searched systematically for PGM using the SEM set at a ×5x magnification for massive sulfide samples and ×200 for disseminated sulfide

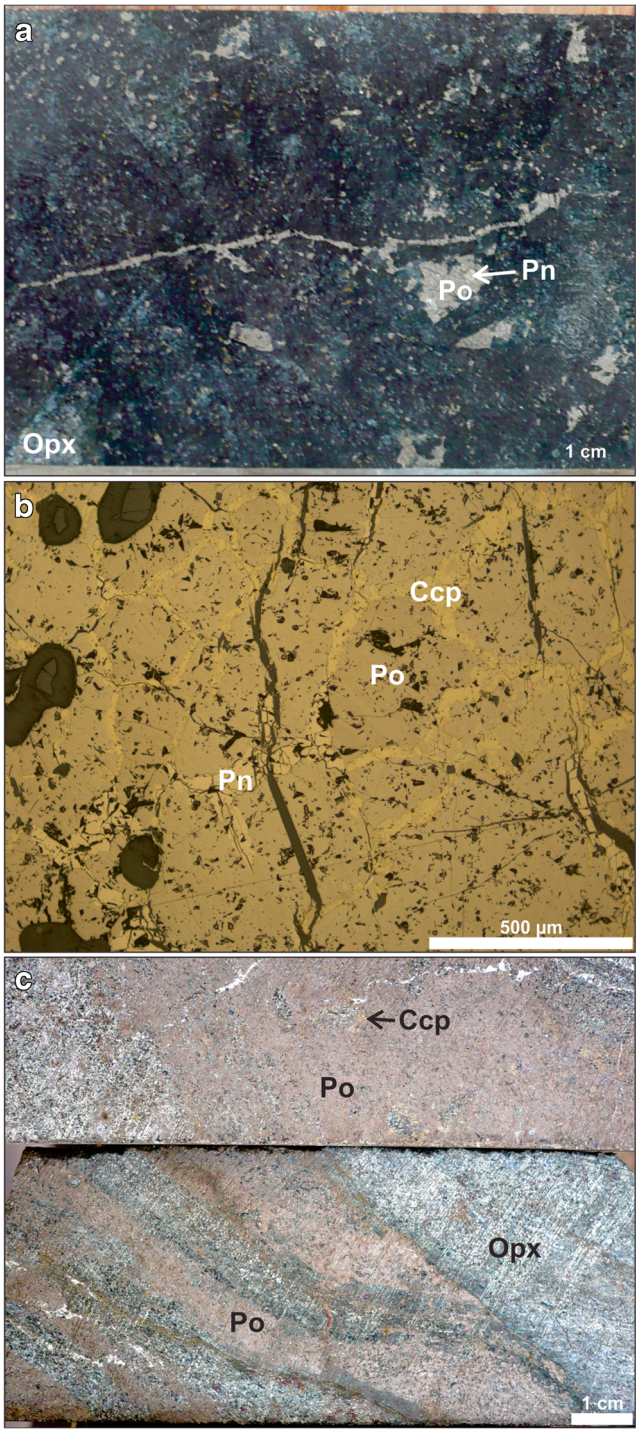

Fig. 4 Examples of ore types from the Limoeiro Ni–Cu–(PGE) deposit. **a** Drill core of a typical disseminated sulfide ore (pyrrhotite (*Po*), pentlandite (*Pn*) and chalcopyrite (*Ccp*)) hosted in orthopyroxenite. **b** The honeycomb-like texture showing chalcopyrite and pentlandite ribbons surrounding polygonal pyrrhotite grains in 120° triple junctions. **c** Drill core of sample 004-115.80, an example of tectonically mobilized and sheared massive sulfide. In this case, the massive sulfide has numerous ellipsoidal elongated silicate inclusions forming a typical "Durchbewegung" texture (term coined by Vokes 1969) suggesting plastic transport of massive sulfide

samples. Quantitative analyses of the larger PGM (>5×5 μm) were obtained by X-ray emission spectrometry using an Oxford Instruments INCA Energy Dispersive X-ray spectrometer attached to the SEM. Operating conditions for the analyses were 20 keV accelerating voltage, with a beam current of ~1 nA, and a working distance of 25 mm (this is important to give a suitable efficient dead time for the detector between 40 and 45 %). A cobalt reference standard was regularly analyzed in order to check for any drift in the analytical conditions. A wide-ranging set of standards obtained from MicroAnalysis Consultants Ltd (St Ives, Cambridgeshire) was used to calibrate the EDX analyzer.

In order to measure the PGE and other trace element contents in BMS, 26 grains from 4 polished thin sections were analyzed, representing massive sulfide orebodies from distinct parts of the intrusion. Laser-ablation ICP-MS analyses were carried out using a New Wave Research UP213 Nd:YAG 213 nm UV laser system coupled to a Thermo X Series 2 ICP-MS. The relative abundances of PGE and other elements were recorded in time-resolved analysis mode (time slices of ~250 ms) as the laser beam followed a line designed to sample single or multiple sulfide phases. The laser beam diameter was 30 μm, with a frequency of 10 Hz and a power of ~6 J cm^{-2}. The sample was moved at 6 μm s^{-1} relative to the laser along a pre-determined line pattern. Ablations were carried out under a pure helium atmosphere (flow ~0.7 L min^{-1}) and the resulting vapor combined with argon (flow rate 0.65–0.75 L min^{-1}) before delivery into the ICP-MS. Acquisitions lasted between 80 and 400 s, including a 20-s gas blank prior to the start of the analysis and a 10-s washout at the end. Signals within the time spectra that could be attributed to PGM included in the sulfides were not selected for integration so the data reflect concentrations in the sulfide minerals alone. Sulfur concentrations were measured prior to LA-ICP-MS using SEM and ^{33}S was used as internal standard. Subtraction of gas blanks and internal standard corrections were performed using Thermo Plasmalab software.

More details on sampling and analytical methods, which include standards, precision and accuracy for each method, can be found in the Electronic supplementary materials (ESM) 1 and 2.

Results

Platinum-group mineralogy

The Limoeiro Ni–Cu–(PGE) sulfide deposit PGM assemblage comprises mostly bismuthotelluride minerals, dominated by Pt–Ni-bearing merenskyite [$(Pd,Pt,Ni)(Te,Bi)_2$]. The massive sulfide ore is dominated by merenskyite which accounts for 98 % of PGM grains observed, whereas the disseminated sulfide ore has a more diverse PGM assemblage (ESM 3). Other

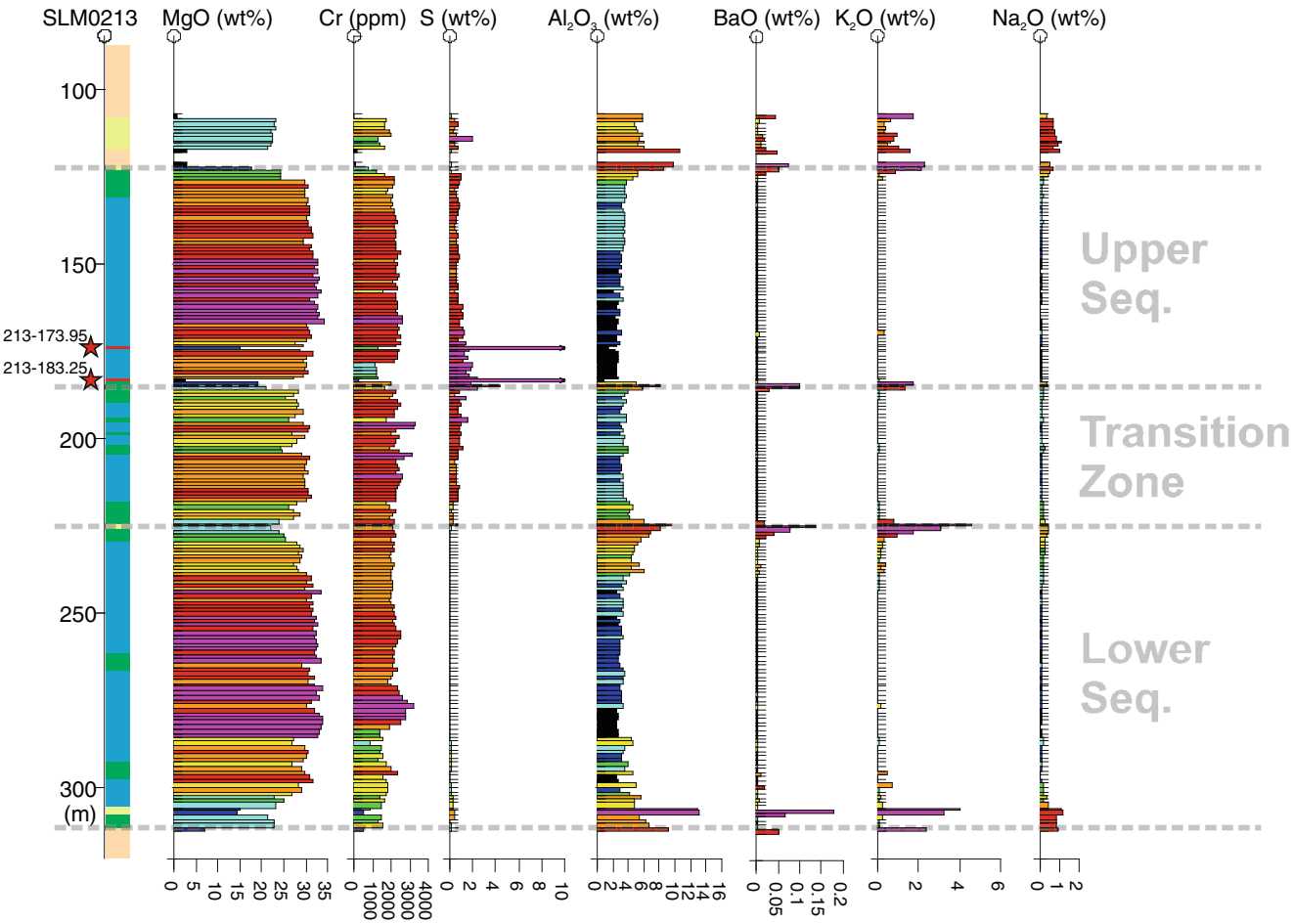

Fig. 5 Representative diamond hole log of the Retiro area. The massive sulfide horizons sampled are marked with a *red star* and labeled with the sample name. The colors for the lithologies are the same as those used in Fig. 3

common PGM are sperrylite ($PtAs_2$), kotulskite [Pd(Te, Bi)], moncheite [$Pt(Te,Bi)_2$], Pt/Pd-bearing melonite [$(Ni, Pt,Pd)(Te,Bi)_2$], an unknown Pd–Pb telluride, hollingworthite [(Rh,Pt,Pd)AsS], an unknown Pd–Ag bismuthotelluride, and cooperite (PtS). The total PGM assemblage identified (ESM 3) is composed of 87 % bismuthotelluride, 8 % arsenide, 1.5 % telluride, 1.5 % sulfarsenide, and a combined 2 % of sulfide, bismuthide, and Sn-PGM (Table 1). Merenskyite accounts for 50 % of the total number of PGM grains in the disseminated sulfide ore, but represents only 45 % by area, mainly because sperrylite and kotulskite have a slightly larger average grain size (Fig. 7). The largest grain is a 5000-μm^2 merenskyite in massive sulfide ore, and the smallest PGM found in this study is a 0.1-μm^2 cooperite that occurs together with a sperrylite as a composite grain. The median PGM grain size is 6.4 μm^2 in nine samples in disseminated ore (×200 search parameter) and 88 μm^2 in six samples of massive ore (×50 search parameter). As merenskyite and sperrylite are the most abundant PGM identified (84 %), their mineralogical characteristics are described in individual sections as follows.

Merenskyite, $(Pd,Pt,Ni)(Te,Bi)_2$

Merenskyite has a wide range of compositions with varying Pt and Ni contents and distinct Te/Bi weight ratios (Table 1). It usually displays euhedral to subhedral forms, occasionally with conspicuous cleavage parallel to the longer crystal axis (Fig. 8a, c, and d). The grains have a dominantly homogeneous composition and can occur as composite grains together with hessite (Ag_2Te), altaite (PbTe), and moncheite. The association with hessite is especially frequent in sample 004-115.80 with ~85 % of the merenskyite grains associated with hessite. This sample is a narrow mobilized and sheared massive sulfide layer composed of sulfide stringers aligned parallel to the deformation fabric, marked by the elongation of amphibole and phlogopite (Fig. 4c). In contrast, non-sheared massive sulfide samples have only ~2 % of the merenskyite grains associated with hessite.

Sperrylite, $PtAs_2$

The second most abundant PGM, sperrylite, occurs as small (median of 25 μm^2 in area) homogeneous grains. The

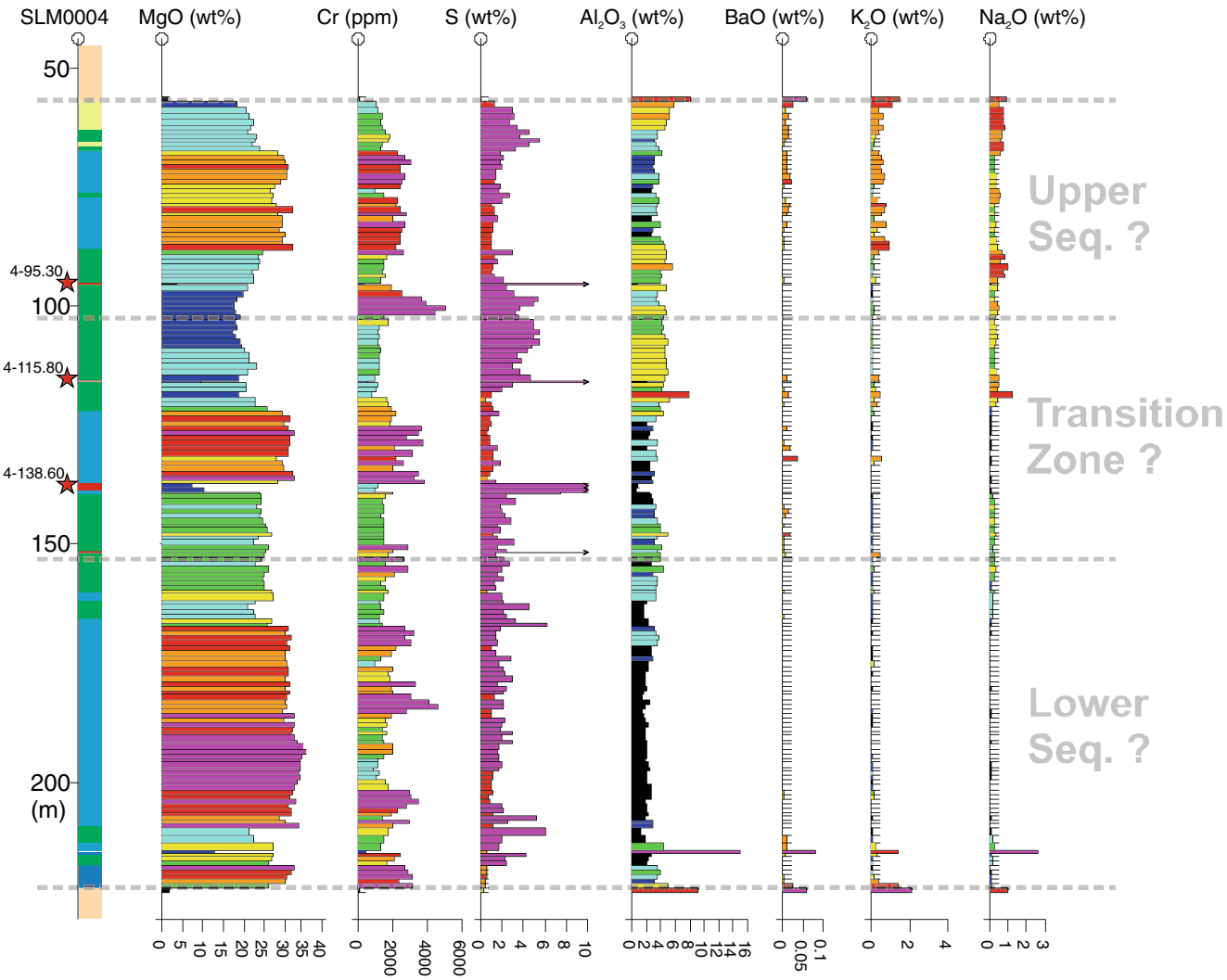

Fig. 6 Representative diamond hole log of the east part of the Piçarra area. The massive sulfide horizons sampled are marked with a *red star* and labeled with the sample name. The colors for the lithologies are the same as those used in Fig. 3

sperrylite varies in form from euhedral diamond shapes to subhedral and more rarely as almost rounded grains (Fig. 9). These sperrylites occasionally contain small amounts of Rh, Cu, Au, and S (Table 1). Rhodium, S, and Cu have been documented in low concentrations in sperrylite elsewhere (Cabri 2002); however, the presence of these elements in the analyses presented here may also be related to other phases below the section. This possibility is particularly likely for S and Rh as occasionally sperrylite forms composite grains with cooperite (Fig. 9b) and hollingworthite in the Limoeiro deposit. Pt-bearing melonite also occurs in composite grains with sperrylite (Fig. 9e). Sperrylite commonly occurs in clusters, and importantly never occurs close to the most abundant PGM, merenskyite.

Platinum-group mineral associations and textures

The PGM in the massive sulfide ores occur mainly associated with pyrrhotite, but associations with silicates are also very common (Fig. 10). This association with silicates reflects the preference of PGM to crystalize at BMS margins or enclosed in BMS but attached to inclusions of rounded (probably spherical) grains composed of serpentine, hornblende, carbonate, chlorite, and other silicates (Fig. 8a, b). One of these silicates either completely fills the spherical inclusion (as observed in two dimensions) or several silicates occur within a single inclusion. Chalcopyrite, pentlandite, and oxides contain far fewer PGM. Sample 004-115.80, which is from a mobilized narrow stringer sulfide layer, is different from the primary massive sulfide samples because the PGM are located in contact with chalcopyrite, pyrrhotite, and silicates, but not with pentlandite or oxides.

In contrast, the silicate minerals in disseminated sulfide ores are the most common host for the PGM. This preference is followed by the occurrence of PGM in order of decreasing abundance in oxides, pyrrhotite, chalcopyrite, and pentlandite (Fig. 10). This pattern underpins the observation that the PGM, despite having a close spatial relationship with BMS,

Table 1 Selected representative quantitative analyses of the PGM found in the Limoeiro deposit

Sample	Litho	Grain No.	Mineral	Fe (wt%)	Ni (wt%)	Cu (wt%)	Rh (wt%)	Pt (wt%)	Pd (wt%)	Au (wt%)	S (wt%)	As (wt%)	Te (wt%)	Bi (wt%)	Total (wt%)
055-228	HZ	5.1	Kotulskite	0.78	4.79			0.89	30.80				40.84	21.71	99.80
002-125	PX	20	Kotulskite						43.55				45.54	10.86	99.95
213-185.00	PX	7	Melonite	3.37	12.88			3.54	7.05				63.94	10.07	100.85
055-228	HZ	2	Merenskyite	1.39	4.46			5.85	22.63				43.23	22.47	100.04
055-228	HZ	6	Merenskyite		8.06			4.31	19.32				44.95	23.77	100.41
055-228	HZ	5.2	Merenskyite		0.49				24.83				32.67	41.88	99.87
004-115.80	MS	3	Merenskyite						25.09				33.77	40.07	98.93
004-115.80	MS	4	Merenskyite						24.97				33.42	40.98	99.37
004-138.60	MS	51	Merenskyite	1.38	3.82			3.86	18.43				54.44	17.90	99.83
004-138.60	MS	18	Merenskyite	0.44	3.74			4.11	18.82				53.39	19.12	99.62
004-95.30	MS	10	Merenskyite		0.64			7.34	22.11				52.10	17.73	99.91
004-95.30	MS	18	Merenskyite		0.79			6.92	21.84				51.18	18.57	99.29
021-137	MS	19	Merenskyite		2.15			8.74	17.39				47.73	23.00	99.00
021-137	MS	6	Merenskyite		2.74			7.29	17.91				50.31	22.34	100.59
213-173.95	MS	7	Merenskyite	0.72	4.68			10.26	12.20				52.78	11.79	99.47
213-173.95	MS	6	Merenskyite	0.85	5.22			10.84	11.94				53.59	18.07	100.51
213-183.25	MS	11	Merenskyite		3.23			8.87	15.83				48.28	23.98	100.19
213-183.25	MS	32	Merenskyite		3.25			10.56	15.74				49.17	22.11	100.83
002-125	PX	4	Merenskyite					1.62	27.66				62.09	8.00	99.37
021-090	AT	22	Michenerite	0.90	0.62				23.88				28.16	46.34	99.90
021-090	AT	20	Michenerite	0.74					24.30				27.55	47.32	99.91
004-110	AT	3	Moncheite	0.87				26.31	10.64				55.26	6.80	99.88
002-125	PX	5	Moncheite					39.57	2.37				54.52	3.72	100.17
002-125	PX	6	Moncheite					43.27					55.41		98.67
213-185.00	PX	67	Moncheite	0.69	0.82			40.98					54.49	3.39	100.38
055-228	HZ	24	Sperrylite			0.71		55.92			0.43	41.98			99.03
002-125	PX	1	Sperrylite					57.57				43.41			100.97
213-185.00	PX	3	Sperrylite				0.78	57.06				42.45			100.29
213-185.00	PX	4	Sperrylite				1.41	56.53				42.41			100.35
213-185.00	PX	29	Sperrylite					56.16		1.75	1.14	40.92			99.96

Lithological unit abbreviations: *AT* amphibolite, *PX* orthopyroxenite, *HZ* harzburgite, *MS* massive sulfide

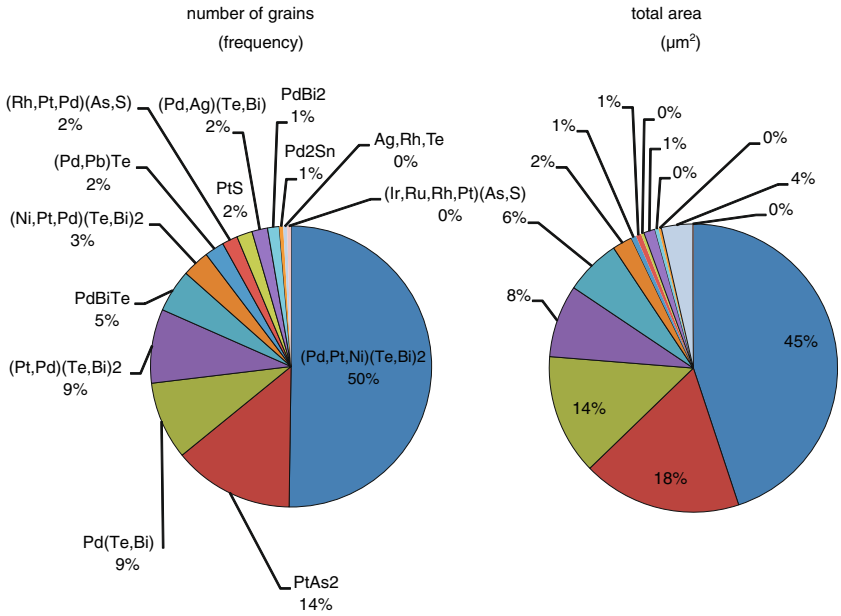

Fig. 7 Pie charts showing the PGM frequency and area abundances in the disseminated ore from the Limoeiro Ni–Cu–(PGE) sulfide deposit

are commonly situated in contact with other phases. Sperrylite is preferentially hosted by oxides (Fig. 10), partly because the most sperrylite-rich sample 213-185.00 is a magnetite-rich orthopyroxenite (ESM 3). It is also shown that the group of less common PGM (classified as "others") has a preferential association with chalcopyrite (Fig. 10).

These patterns of association of the PGM described above are related to different textures and fabrics. The most common

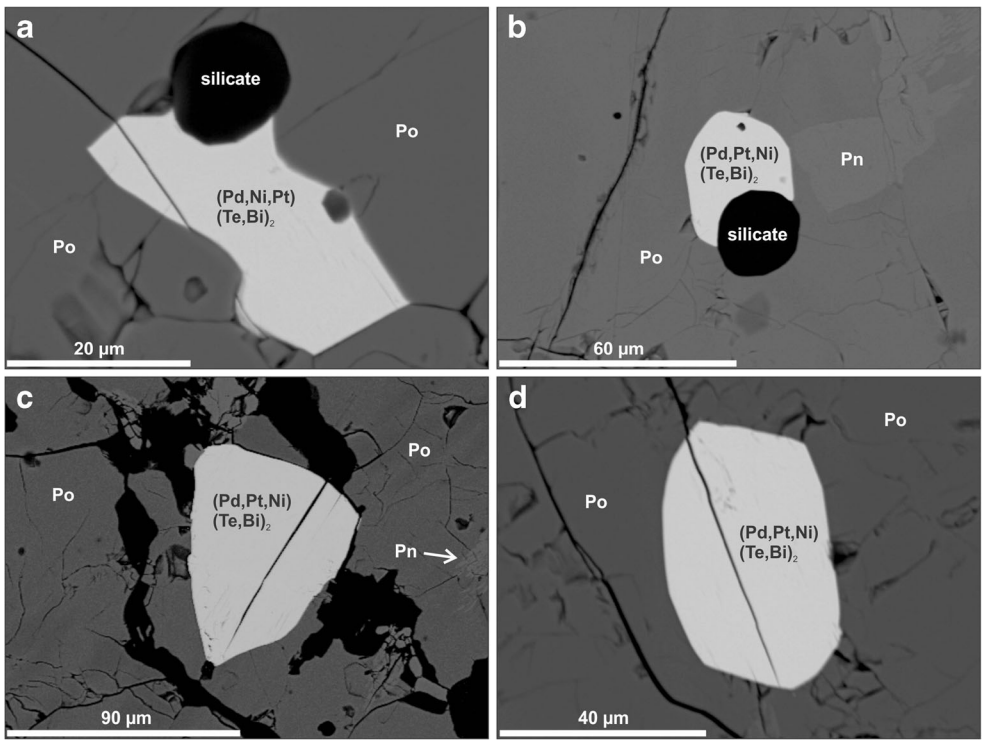

Fig. 8 Back-scattered electron images of: **a** Subhedral merenskyite grain with discrete cleavage, enclosed by pyrrhotite (*Po*), and attached to a rounded silicate in massive sulfide ore, sample 213-173.95, grain No. 3. **b** Euhedral merenskyite grain enclosed by pyrrhotite and pentlandite (*Pn*) and attached to a rounded silicate in massive sulfide ore, sample 213-183.25, grain No. 6. **c** Subhedral merenskyite grain with clear cleavage parallel to the longer crystal axis, enclosed by pyrrhotite, surrounded by open fractures in massive sulfide ore, sample 213-183.25, grain No. 12. **d** Subhedral merenskyite grain with discrete cleavage parallel to the longer crystal axis, enclosed by pyrrhotite, and affected by a fracture through the massive sulfide ore, sample 213-173.95, grain No. 10. Mineral abbreviations from Whitney and Evans (2010)

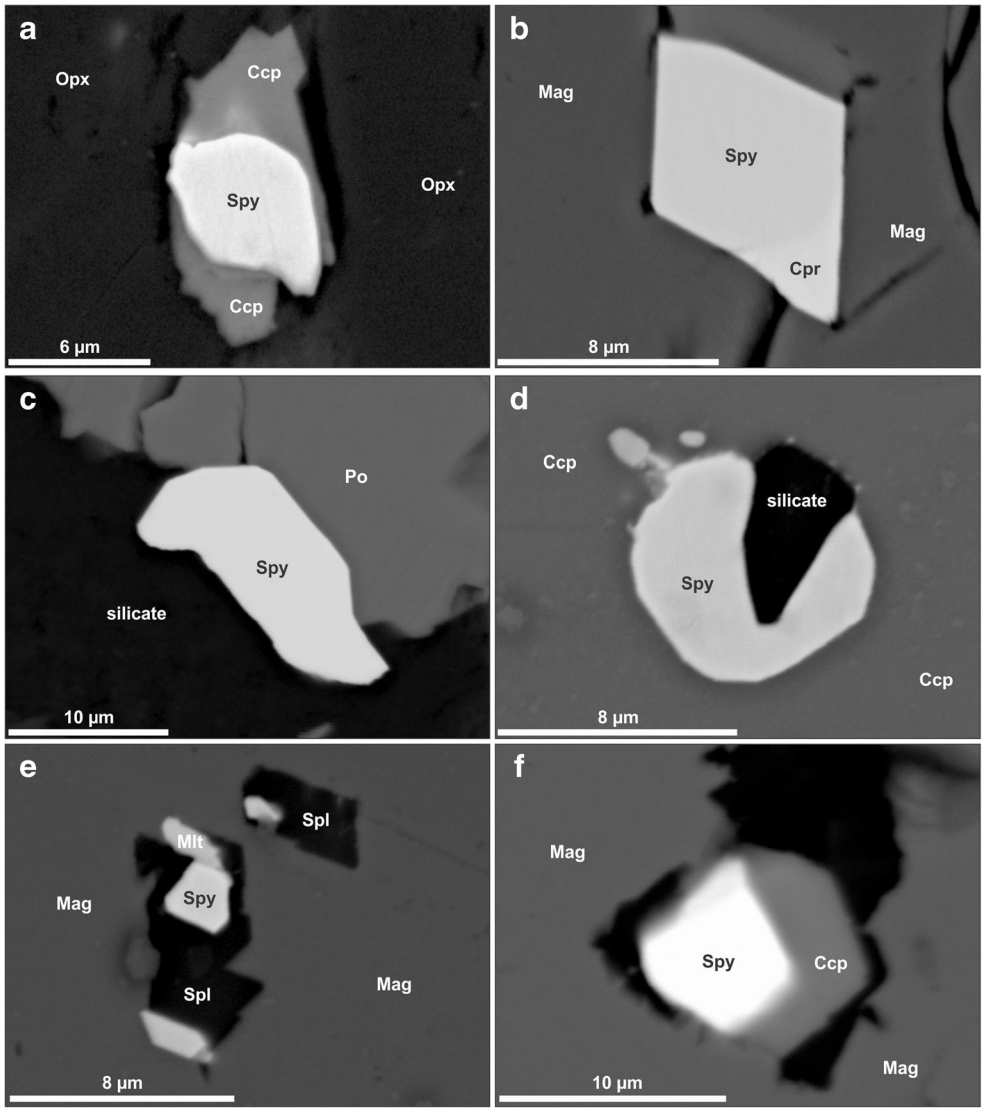

Fig. 9 Back-scattered electron images of: **a** Subhedral sperrylite (*Spy*) in contact with and partially surrounded by chalcopyrite (*Ccp*), both enclosed by silicate forming an orthopyroxenite containing disseminated sulfides, sample 213-185.00, grain No. 35. **b** Euhedral sperrylite with a typical diamond shape, forming a composite grain with cooperate (*Cpr*), both enclosed by magnetite (*Mag*) in an orthopyroxenite containing disseminated sulfides, sample 213-185.00, grain No. 3. **c** Subhedral sperrylite at the contact between BMS and a silicate in an orthopyroxenite containing disseminated sulfides, sample 002-125, grain No. 1. **d** Anhedral to subhedral sperrylite in contact with a silicate, both enclosed by chalcopyrite in an orthopyroxenite containing disseminated sulfides, sample 213-185.00, grain No. 29. **e** Euhedral sperrylite forming a composite grain with melonite (*Mlt*), both included in a spinel (*Spl*) grain (probably derived during metamorphism of chromite) in an orthopyroxenite containing disseminated sulfides, sample 213-185.00, grain No. 21. **f** Euhedral sperrylite in contact with chalcopyrite, both enclosed by magnetite in an orthopyroxenite, sample 213-185.00, grain No. 11. Mineral abbreviations from Whitney and Evans (2010), Kretz (1983), and Spear (1993)

textures identified are (i) PGM on the margin of BMS, (ii) enclosed by the BMS, and (iii) enclosed by silicate or oxide minerals. Less common textures are (iv) PGM in sulfide veinlets, (v) on the edge of BMS but where PGM show irregular reaction boundaries with the adjacent mineral phase, and (vi) elongate PGM associated with sulfides within silicate cleavages (Fig. 11). Compared with disseminated ores, massive sulfides have more abundant PGM enclosed by BMS. In contrast, PGM enclosed by silicates or oxides are much more frequent in disseminated ores (Fig. 11).

The distributions of merenskyite and sperrylite in each of the distinct textural types also show a pattern (Fig. 12). Sperrylite occurs mainly enclosed by silicate or oxide and less frequently at the margin of BMS or more occasionally enclosed by BMS. Merenskyite occurs in all these textual settings but is most frequently enclosed by BMS and unlike sperrylite also occurs in sulfide veinlets, with irregular reaction boundaries and as elongate crystals associated with sulfides within silicate cleavages (Fig. 12).

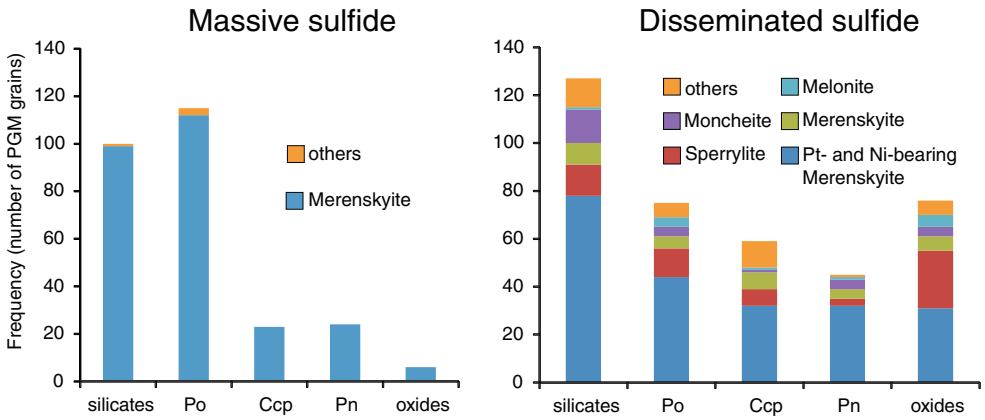

Fig. 10 Bar charts showing the frequency of each mineral phase in contact with the PGM from the Limoeiro Ni–Cu–(PGE) sulfide deposit

BMS that encloses PGM occurs either as sulfide blebs included within primary silicate minerals (Fig. 13a) or as interstitial minerals between cumulus silicates (Fig. 13b). Although it is common to find PGM enclosed by BMS in massive sulfide ores in the Retiro area, they are also commonly in contact with rounded silicate inclusions (Fig. 8a, b). The PGM that are situated on the edges of BMS grains have euhedral to subhedral forms and their grains commonly cross BMS boundaries and extend into adjacent mineral phases (silicates of magmatic or high-grade metamorphic origin; Figs. 9c and 13c, d). PGMs on the margins of BMS grains frequently have an irregular contact with the adjacent mineral phase, which suggests a reaction relationship between the phases. In such cases, it is common for the PGM to be associated with hessite-forming composite grains. This texture commonly occurs where the PGM is in direct contact with low-grade metamorphic or hydrothermal minerals, such as antigorite (Fig. 13e). It also occurs where primary sulfide blebs within orthopyroxene grains have been affected by late-magmatic or hydrothermal sulfide remobilization (Fig. 13f). The PGM located within chalcopyrite or pentlandite veinlets generally occupy the whole width of the veinlet and generally have irregular forms and crosscut the primary pyrrhotite and silicate grains (Fig. 13g) or take the place of pre-existing fractures in magnetite (Fig. 13h). PGM within sulfides filling spaces in silicate cleavages occur hosted in primary orthopyroxene grains (Fig. 13i) whether they are deformed or not and also in high-grade metamorphic amphibole (Fig. 13j). PGM enclosed by silicates or oxides can be surrounded by primary mineral phases (Figs. 9e and 13k) or by low-grade metamorphic or hydrothermal minerals, such as antigorite (Fig. 13l). In these cases, the PGM are not in direct contact with the BMS but are still in close proximity.

Merenskyite compositional variation

Merenskyite ($PdTe_2$) occurs in continuous solid solution with melonite ($NiTe_2$) and moncheite ($PtTe_2$; Barkov et al. 2002; Cabri 2002). Merenskyite grains within any individual massive sulfide ore sample have a very similar, homogeneous composition, but merenskyite in massive sulfide ores shows a systematic variation throughout the chonolith that hosts the Limoeiro deposit. Merenskyite within the mineralized upper sequence is richer in Pt and Ni in the west (Retiro; most primitive) but is richer in Pd in the east (Piçarra; most fractionated),

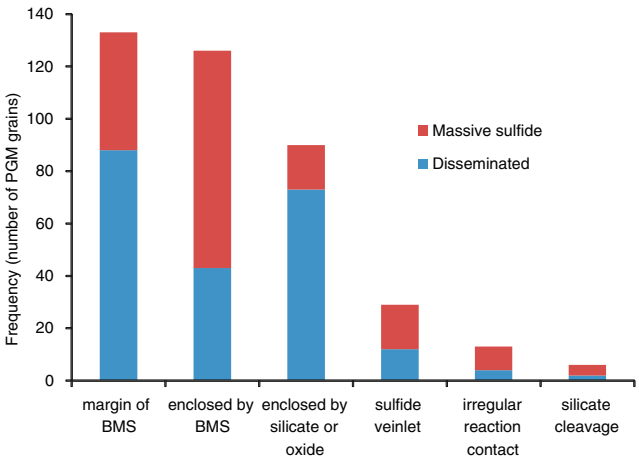

Fig. 11 Bar chart showing the frequency of PGM in different textural sites in the Limoeiro Ni–Cu–(PGE) deposit

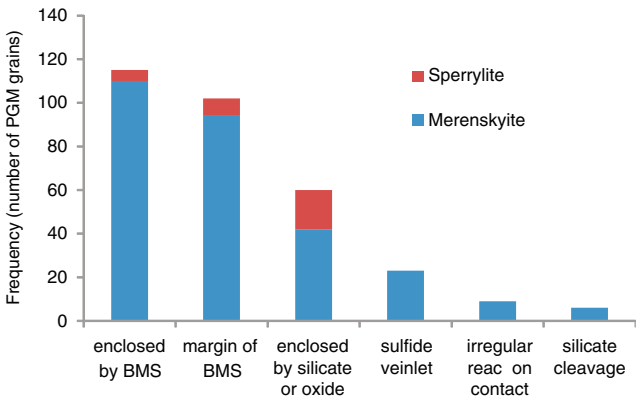

Fig. 12 Bar chart showing merenskyite and sperrylite abundances for each texture in the Limoeiro Ni–Cu–(PGE) deposit. These minerals are the two most abundant PGM phases in the Limoeiro deposit

ranging from $(Pd_{0.42},Ni_{0.33},Pt_{0.21},Fe_{0.06})(Te_{1.64},Bi_{0.33})$ to $(Pd_{0.84},Pt_{0.15},Ni_{0.03})(Te_{1.65},Bi_{0.33})$ (Fig. 14). A different composition, poorer in Pt and/or Ni, occurs in mobilized massive sulfide in the transition zone in the Piçarra area, ranging from $(Pd_{1.02})(Te_{1.14},Bi_{0.84})$ to $(Pd_{0.90},Fe_{0.13},Ni_{0.07})(Te_{1.46},Bi_{0.44})$ (Figs. 4c and 14).

The Te/Bi atomic ratio does not show a change between the most primitive and most fractionated primary massive sulfide samples, although the merenskyite analyses from the sheared massive sulfide sample (004-115.80) are considerably more Bi rich and form a separate cluster of plots on the Te/Bi biplot (Fig. 15).

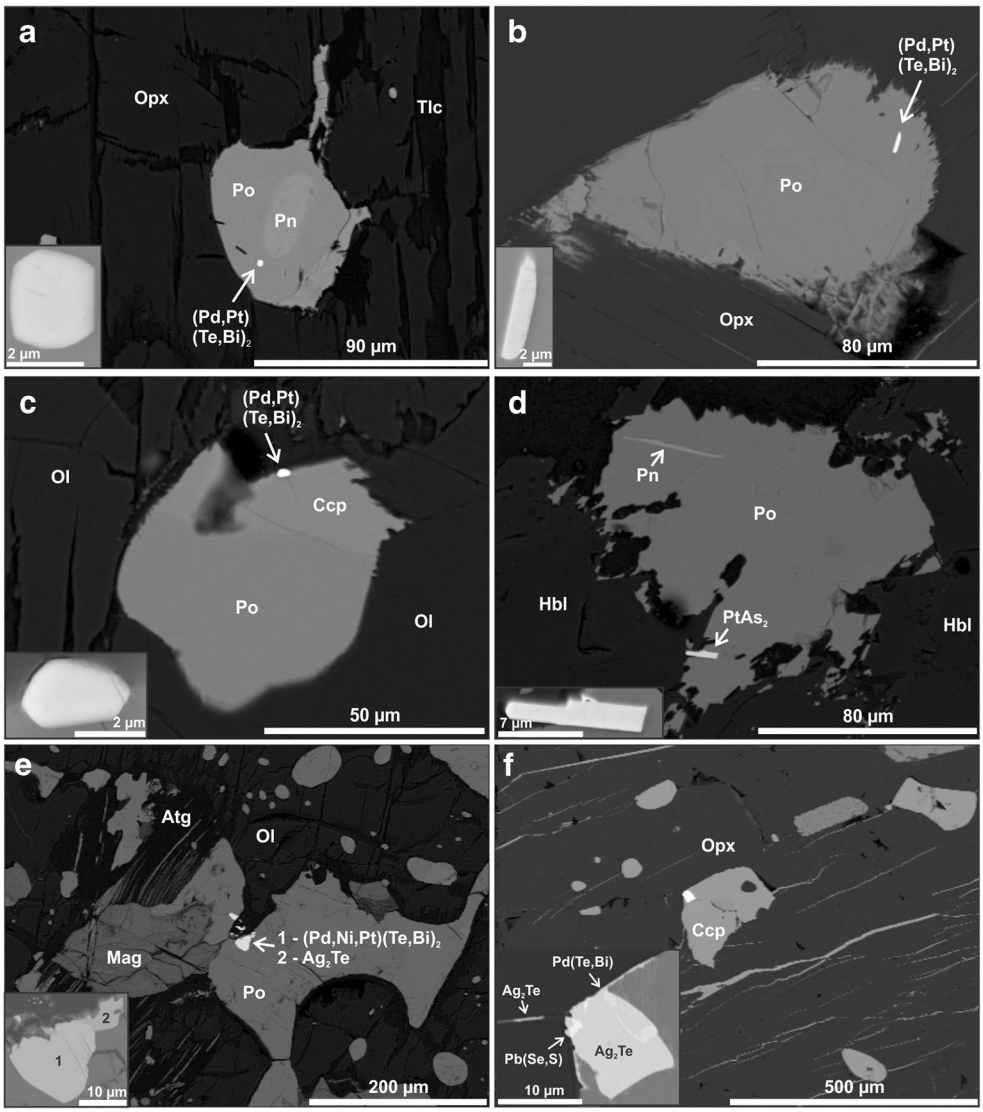

Fig. 13 Back-scattered electron images of: **a** An euhedral merenskyite enclosed by a BMS bleb included in an orthopyroxene (*Opx*), itself partly altered to talc (*Tlc*), in sample 018-155, grain No. 9. **b** An elongate merenskyite enclosed by a partly remobilized intercumulus BMS surrounded by orthopyroxene grains in sample 004-087, grain No. 14. **c** A subhedral merenskyite located between a BMS bleb surrounded by olivine that is partly serpentinized in sample 018-155, grain No. 17. **d** A subhedral elongate sperrylite (*Spy*) crystallized on the edge of a pyrrhotite (*Po*) and in contact with metamorphic hornblende (*Hbl*) in sample 002-125, grain No. 25. **e** A composite grain (merenskyite+hessite) at the edge of a pyrrhotite showing an irregular corroded contact with antigorite (*Atg*) in sample 021-137, grain No. 6. **f** A composite grain (merenskyite+hessite) at the edge of a chalcopyrite (*Ccp*) bleb showing an irregular corroded contact with the host orthopyroxenite that is itself crosscut by several veinlets containing remobilized sulfide in sample 213-185.00, grain No. 30. Mineral abbreviations from Whitney and Evans (2010), Kretz (1983), and Spear (1993). **g** A merenskyite grain within a pentlandite (Pn)-filled veinlet in sample 021-137, grain No. 1. **h** A merenskyite grain within a pentlandite-filled veinlet that occupies a fracture crosscutting a magnetite (Mag) grain in sample 213-185, grain No. 66. **i** An elongate merenskyite grain within Po situated in Opx cleavage in sample 004-087, grain No. 12. **j** An elongate merenskyite grain with Ccp located in a metamorphic Hbl cleavage in sample 004-067, grain No. 1. **k** An euhedral composite grain (Spy+melonite (*Mlt*)) enclosed by orthopyroxene in sample 213-185, grain No. 33. **l** An elongate merenskyite grain enclosed by Atg in sample 055-228, grain No. 10

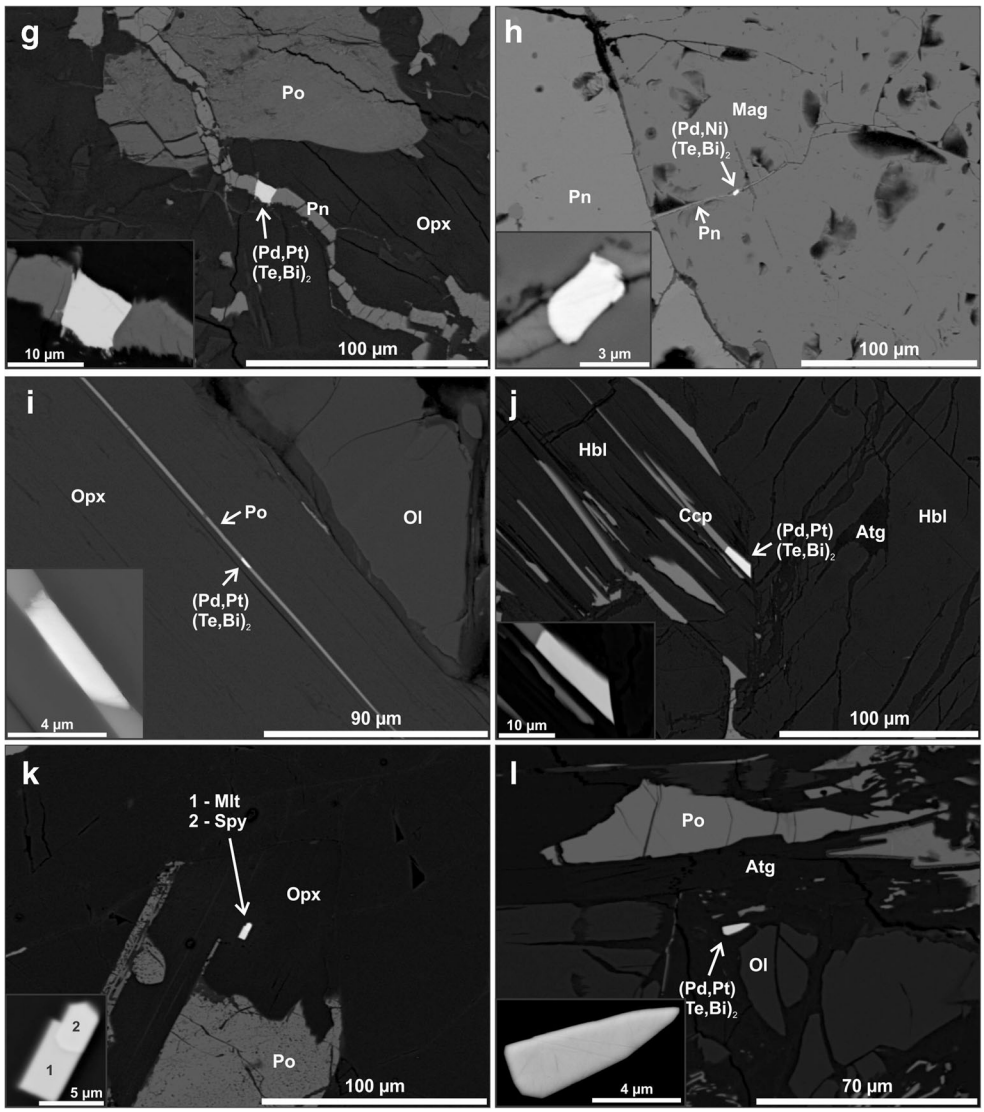

Fig. 13 (continued)

Two merenskyite grains in primary massive sulfide sample 021-137 have similar compositions to the merenskyite grains in sheared massive sulfide sample 004-115.80. These two particular grains are hosted within a chalcopyrite veinlet that crosscuts silicates. Merenskyite in disseminated sulfides is compositionally very variable within any individual sample, and no trends or systematic changes in compositions could be identified between different parts of the chonolith.

PGE in the base metal sulfide

PGE, other associated metals, and their most important ligands (e.g., Te, Bi, As, S, Sb, Se) were analyzed in pyrrhotite, pentlandite, and chalcopyrite in the massive sulfide samples from the Limoeiro deposit. Several elements were shown to have concentrations below the lower limits of detection (LLD) of the analytical method and some others show great variability between analyses (Table 2). Palladium and Co are concentrated in pentlandite with ~6 ppm and ~1.2 wt%, respectively. Zinc, Ag, and Cd are most concentrated in chalcopyrite>pentlandite~pyrrhotite. Concentrations of Pt, Ir, Os, Ru, and Rh are mainly below LLD. Based on the few analyses above the LLD, Ru and Rh are present in solid solution, as micronuggets or nanonclusters (see, Helmy et al. 2013) in BMS, mostly in pentlandite. Pt, Ir, and Os occur in pyrrhotite and pentlandite, but not in chalcopyrite. Cobalt, Pd, Zn, Ag, Cd, Pt, Ir, Os, Ru, and Rh are concentrated in the Piçarra BMS rather than in Retiro BMS. Selenium has similar values for all three BMS and constant concentrations in the two different orebodies. Bismuth is more concentrated in chalcopyrite, and it seems to be the only trace element that is more concentrated in the Retiro BMS compared with the Piçarra BMS. No specific BMS can be identified as the main host of tellurium, probably because its concentration is close to lower detection limit in most of analyses.

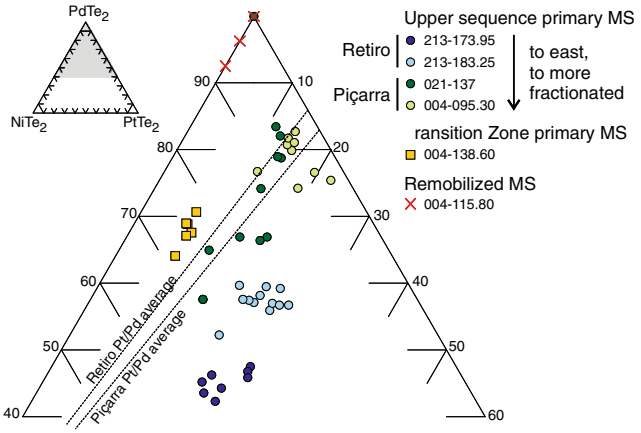

Fig. 14 Compositional variation of PGM belonging to the solid solution series of melonite, merenskyite, and moncheite in the Limoeiro Ni–Cu–(PGE) sulfide deposit. Results of 60 analyses are projected onto the Ni–Pd–Pt ternary diagram (atomic proportions). The *dashed line* indicates the average Pt/Pd atomic ratio for the two main Limoeiro deposit targets. *MS* massive sulfide

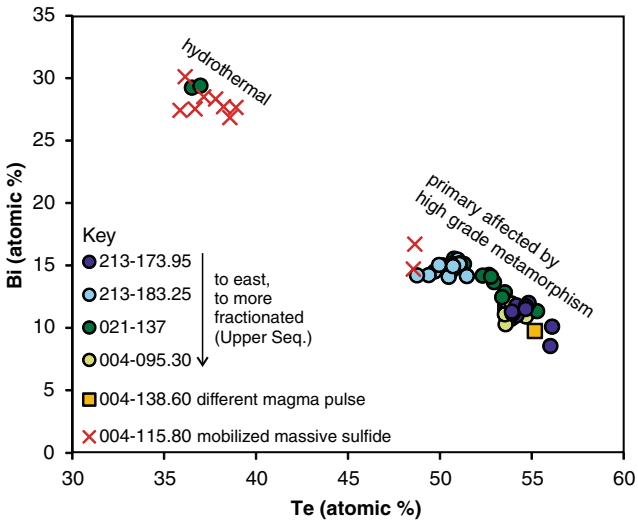

Fig. 15 Compositional Te and Bi variation of 60 merenskyite grains in the Limoeiro Ni–Cu–(PGE) sulfide deposit. *MS* massive sulfide

Mass balance calculation

A mass balance calculation was carried out to determine which of the BMS concentrates each of the PGE and to determine the total amount of PGE in BMS. This mass balance must be regarded as an approximation because of the limited representativeness of the small sample contained in the thin sections relative to the bulk deposit mineralogy, relatively large analytical uncertainties, and high variability of metal content in each of the BMS minerals.

The relative abundances of the BMS are essential to the mass balance calculation, as each of them has a distinct PGE content. Using the Votorantim Metals drill core assay database, tenors (normalization to 100 vol.% sulfides) were calculated for the Piçarra and Retiro areas, using the linear correlation of Ni, Cu, Pd, and Pt versus S up to 37 wt% S, which is approximately the expected grade for a rock containing 100 vol.% of magmatic sulfides in Limoeiro (i.e., pyrrhotite>>pentlandite~chalcopyrite>magnetite; Mota-e-Silva et al. 2013). The Limoeiro deposit is essentially composed of a disseminated sulfide (Mota-e-Silva et al. 2013), in which the sulfide content varies from 2 to 55 vol%. Thus using a linear regression of metal data (Ni, Cu, Pd and Pt) versus S is a robust method to calculate tenors (Kerr 2001). Typical and generic compositions for BMS were used, as the Limoeiro BMS compositions were not determined. All Cu and Ni were allocated in chalcopyrite and pentlandite respectively and the remainder of the S was used to form pyrrhotite (Naldrett 1981). Therefore tenor and proportions of pyrrhotite, chalcopyrite and pentlandite were calculated for the Retiro and Piçarra areas (Table 3). Multiplying the BMS abundances by the Pd content within the BMS recorded in the LA-ICP-MS analyses, it is possible to calculate how much Pd should be in each of the BMS in a hypothetical rock composed of 100 vol.% magmatic sulfides (Table 3). This value can be compared with the deposit Pd tenor previously calculated. The difference between the two values should be related to the amount of Pd accommodated in discrete PGM grains. The result is that 84–88 % of the Pd is in PGM, and 12–16 % of the Pd is in the BMS (Table 3).

Whole rock chemistry

Piçarra has lower tenors and higher Cu/Pd and Ni/Cu ratios than Retiro (Table 3), which indicates that it formed from a more fractionated silicate magma (Mota-e-Silva and Ferreira Filho unpublished). The whole rock Pt/Pd weight ratio for Piçarra (0.38) is slightly but consistently higher than for the Retiro area (0.33; Fig. 16). Pt and Pd are strongly correlated in both the Retiro (R^2= 0.78) and Piçarra orebodies (R^2=0.88; Fig. 16).

To investigate the samples that fall away from the linear trend line shown in Fig. 16, a plot of MgO versus Pt/Pd ratio has been constructed separating the four different lithologies in the Limoeiro Ni–Cu–(PGE) sulfide deposit (Fig. 17). The vast majority of the whole rock sample plot generally close to the average Pt/Pd ratio for the deposit (0.35), but the amphibolite deviates from most of the other lithologies (higher Pt/Pd ratio). The two samples with the highest Pt/Pd ratios are phlogopite-bearing rocks affected by tectonic deformation.

In contrast, most of massive sulfides have lower Pt/Pd ratios. The two samples that plot below the bottom line (five times less than the average Pt/Pd ratio) are tectonically deformed rocks with mobilized massive sulfide stringers. Sample 004-115.80, which is a typical mobilized massive sulfide (Fig. 4c), has grades of 3.4 ppm Pd and 0.22 ppm Pt with a Pt/Pd ratio of 0.06, similar to the two tectonically deformed rocks with mobilized massive sulfide stringers noted above. Sample 004-115.80 is not plotted on Fig. 17, due to its stratigraphic position in the transition zone.

Table 2 Summary of average and 1 standard deviation of PGE and other metal and semimetal concentrations (in ppm) in the BMS

	Retiro						Piçarra					
	Po (n=4)		Ccp (n=3)		Pn (n=5)		Po (n=4)		Ccp (n=4)		Pn (n=6)	
	Avg.	1σ	Avg.	1σ	Avg.	1σ	Avg.	1σ	Avg.	1σ	Avg.	1σ
^{59}Co	137	147	464	291	9387	478	190	88	840	1241	14,222	597
^{66}Zn	18	7	957	297	53	26	31	30	14,451	23,690	1030	1493
^{75}As	<9		<9		<9		<9		<9		<9.00	
^{82}Se	99	10	94	18	105	12	99	14	104	24	95	15
^{101}Ru[a]	<0.06		<0.06		0.09	0.08	<0.06		<0.06		0.18	0.32
^{103}Rh[a]	<0.09		<0.09		<0.09		<0.09		<0.09		1.19	1.17
^{108}Pd[a]	0.2	0.1	0.4	0.2	5.2	2.7	0.2	0.1	0.6	0.7	7.7	2.0
^{109}Ag	0.3	0.1	<0.3		0.4	0.4	2.6	2.5	6.8	4.6	3.0	3.1
^{111}Cd	<0.7		1.5	1.0	<0.7		<0.7		19.8	28.3	1.9	2.4
^{121}Sb	<0.8		<0.8		<0.8		<0.8		<0.8		<0.8	
^{125}Te	2.8	2.7	2.1	3.0	<0.8		<0.8		2.1	1.6	1.7	1.8
^{185}Re	0.08	0.05	<0.03		<0.03		<0.03		<0.03		<0.03	
^{189}Os	0.12	0.10	<0.02		<0.02		0.19	0.22	<0.02		<0.02	
^{193}Ir	<0.02		<0.02		<0.02		0.14	0.24	<0.02		1.26	2.00
^{195}Pt	<0.02		<0.02		<0.02		<0.02		<0.02		0.11	0.10
^{197}Au	<0.01		<0.01		<0.01		<0.01		<0.01		0.02	0.02
^{209}Bi	0.9	0.7	2.6	1.2	1.3	0.7	0.4	0.3	1.3	0.4	0.9	0.5

The BMS: *Po* pyrrhotite, *Ccp* chalcopyrite, *Pn* pentlandite

[a] The isotopes that were corrected for interferences

Discussion

The role of the primary magma in formation of the PGM

The processes by which PGE are transferred from a magma to a sulfide liquid and subsequently incorporated into monosulfide solid solution (MSS) and/or intermediate solid solution (ISS) have been discussed by Li et al. (1996), Naldrett (2004), Sinyakova and Kosyakov (2007), Helmy et al. (2010), Holwell and McDonald (2010), and Liu and Brenan (2012). PGE-bearing bismuthotellurides in Limoeiro ores are strongly associated with BMS (Fig. 10) mainly situated at the edge of sulfide blebs and intercumulus BMS or completely enclosed by the BMS (Fig. 11). Many other deposits with similar PGM textures have been interpreted to have formed through exsolution of the PGE from BMS during cooling at temperatures <650 °C (Barnes et al. 2008; Prichard et al. 2013). Such a process has been confirmed experimentally (Makovicky et al. 1990; Helmy et al. 2007).

The Limoeiro parental magma was relatively enriched in Te and Bi compared with the other typical PGE ligands (Sb, As, S, and Se), as suggested by the strong dominance of bismuthotellurides (87 %) in the PGM assemblage. This interpretation relies on the fact that BMS are essentially composed of the common magmatic assemblage (pyrrhotite, chalcopyrite, and pentlandite; Mota-e-Silva et al. 2013), and the strong correlations between Pt and Pd (Fig. 16). Additionally, the S/Se ratio varies between 3200 and 3800 (Table 2) in the Limoeiro BMS, which is within the normal mantle range variation (Lorand et al. 2003). This shows that no post-magmatic

Table 3 Calculated Ni, Cu, Pd, and Pt tenors, estimation of BMS proportions in the sulfide fraction, concentration of Pd for each BMS in a 100 vol.% sulfide rock, and the partitioning of Pd between BMS and PGM

	Drilling area	
	Retiro	Piçarra
Ni tenor (wt%)	5.6	3.0
Cu tenor (wt%)	5.7	4.5
Pd tenor (ppm)	8.7	5.5
Pt tenor (ppm)	2.7	2.1
Pyrrhotite (vol.)	67 %	78 %
Chalcopyrite (vol.)	16 %	13 %
Pentlandite (vol.)	16 %	9 %
Pd (ppm) in Po	0.1	0.1
Pd (ppm) in Ccp	0.1	0.1
Pd (ppm) in Pn	0.9	0.7
Pd (ppm) in BMS	1.1	0.9
Pd in BMS	12 %	16 %
Pd in PGM	88 %	84 %

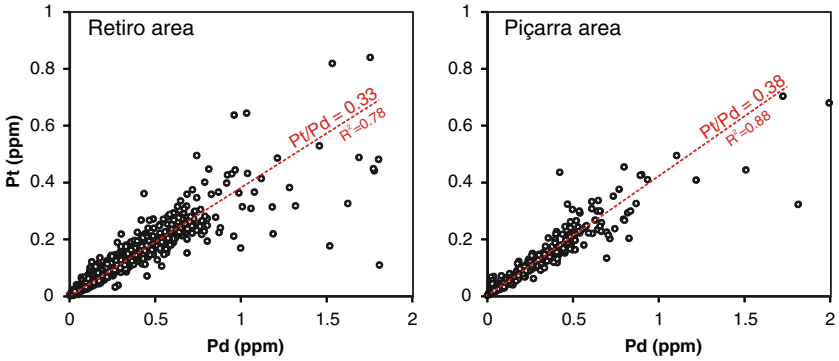

Fig. 16 Whole rock Pt and Pd contents of 2006 samples from the two main areas in the mineralized upper sequence of the Limoeiro Ni–Cu–(PGE) deposit. The linear trend (*red dashed line*) indicates the average Pt/Pd ratio. Data from Votorantim Metals

S-loss or S-gain occurred throughout the Limoeiro deposit. The high-grade metamorphism did not mobilize the chalcogenes, semimetals or metals in the Limoeiro deposit. Thus the ore geochemical characteristics must be interpreted in the light of magmatic processes. It is known that country rock contamination has an influence on the semimetal and metal content in mafic magmas (Ames and Farrow 2007; Hutchinson and McDonald 2008; Godel et al. 2012). In Sudbury, Canada, for example, the PGM assemblage is influenced by the semimetal content in the underlying source rock with As being more abundant on the south side of the complex compared with the northern ranges (Cabri and Laflamme 1976; Ames et al. 2008; Dare et al. 2010a). It has been speculated that the country rock associated with the Limoeiro deposit, a sulfide-bearing paragneiss, could have provided an external source of S for the Limoeiro mafic magma, which is supported by the occurrence of xenoliths of paragneiss in the base of massive sulfide layer (Mota-e-Silva et al. 2013). It is known that Te and Bi have concentrations of the order of ones to tens of ppb in basalts, whereas in sedimentary rocks, especially those derived from carbonaceous sediments, Te and Bi concentrations are in the range of tens of parts per million (Santoliquido and Ehmann 1972; Beaty and Manuel 1973). We consider likely that the paragneiss country rock, which contains several calc-silicate layers, has contaminated the Limoeiro mafic magma with a significant input of Te and Bi, which later formed bismuthotelluride PGM by exsolution from BMS at temperatures <650 °C.

In Limoeiro, the fractionation vector is eastwards (from Retiro in the west to Piçarra in the east; Mota-e-Silva and Ferreira Filho, unpublished). Thus, the ore in samples 213-183.25 and 213-173.95 from Retiro segregated from more primitive silicate magma than those in sample 021-137 from the west part of Piçarra, which is more primitive than sample 004-095.30 from the central part of Piçarra. The orebodies in the most fractionated part in the east have lower tenors of Ni, Cu, Pd, and Pt compared with the ones in the west (Table 3).This geochemical contrast is also recorded in typical geochemical proxies (Ni/Cu and Cu/Pd) used to identify levels of previous sulfide segregation in magmatic systems (Barnes et al. 1993; Barnes and Lightfoot 2005). The Ni/Cu ratio decreases from 0.99 to 0.66, and the Cu/Pd ratio increases from ~6500 to ~8200 to the east (Table 3). It is possible to assume similar R- and N-factors (Naldrett 2004) for the

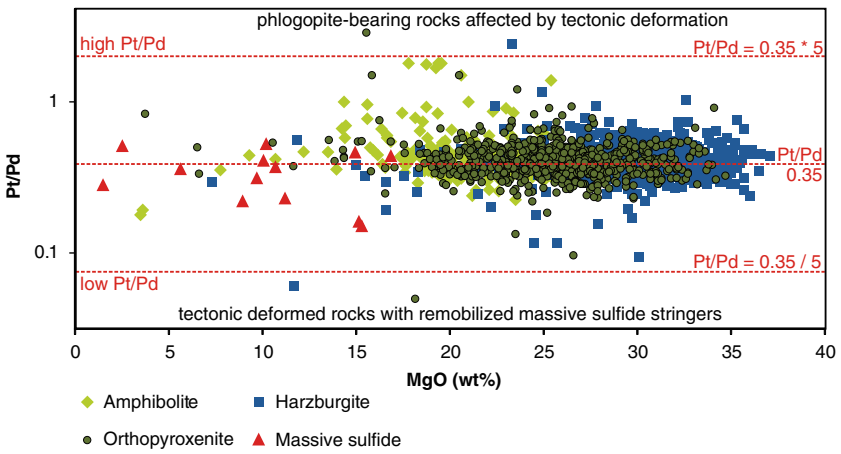

Fig. 17 Whole rock MgO content versus Pt/Pd weight ratio biplot of 2006 samples from different lithologies from the mineralized upper sequence of the Retiro and Piçarra areas in Limoeiro Ni–Cu–(PGE) deposit. The *central red dashed line* represents the bulk deposit average Pt/Pd weight ratio. The *top and bottom red dashed lines* are respectively five times and a fifth of the average Pt/Pd weight ratio and are plotted as a reference for the identification of the samples with relatively high and low Pt/Pd weight ratios. The *text in black* refers to the four samples (two at the top and two at the bottom) that are outside the *red dashed lines*. Data from Votorantim Metals

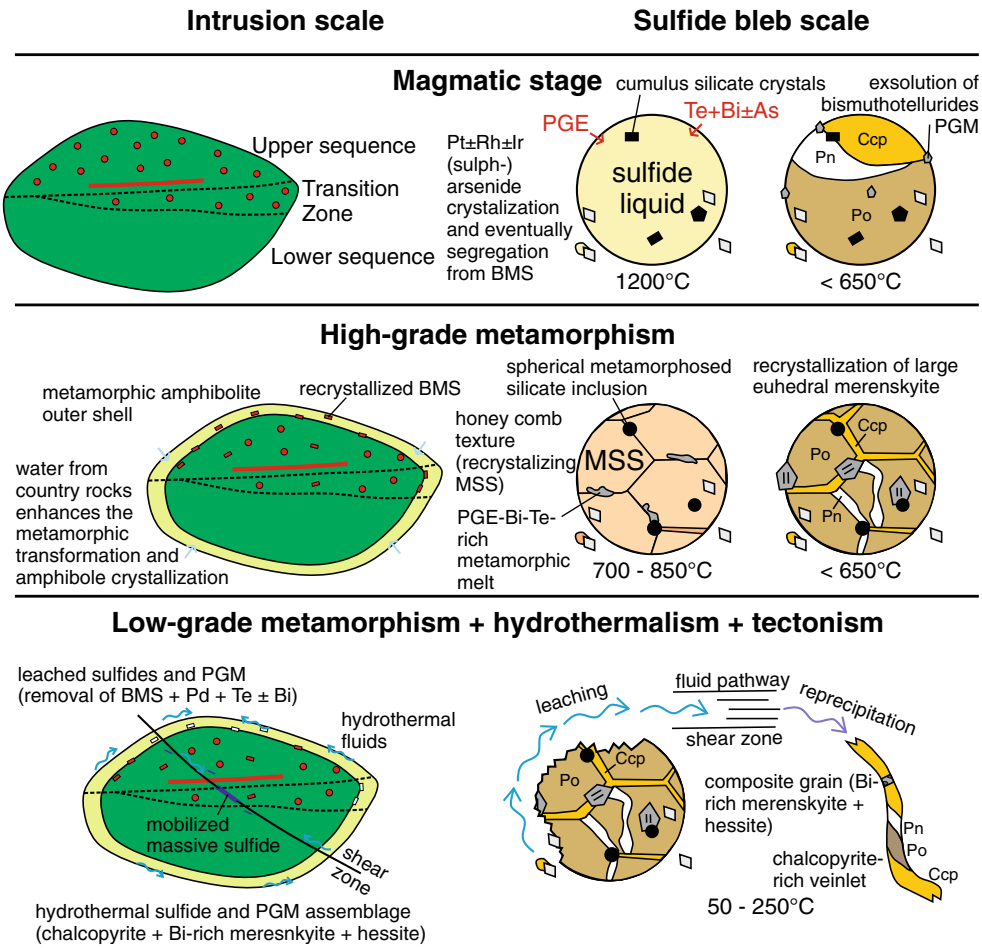

Fig. 18 Schematic model representing the chonolithic Limoeiro intrusion showing an intrusion-scale cross section and small scale chart of magmatic sulfide blebs showing the main geological phases that occurred during the formation of the primary, high-grade metamorphic, and lower temperature alteration secondary sulfide and PGM assemblages in the Limoeiro Ni–Cu–(PGE) sulfide deposit

Piçarra and Retiro orebodies, because they are adjacent portions of the same magma conduit (Fig. 2).

Previous work has shown the existence of a continuous solid-solution series between merenskyite and melonite and between merenskyite and moncheite (Garuti and Rinaldi 1986; Hudson 1986; Harney and Merkle 1990). Compositions containing all three members (merenskyite, melonite, and moncheite), including one analysis with exactly equal proportions of each have been observed in the Wellgreen Ni–Cu–PGE deposit, Canada (Barkov et al. 2002). The minerals in that study consist of members of the merenskyite–moncheite series, which are relatively enriched in melonite (10 to 30 mol.%). In contrast, in Limoeiro the grains have compositions lying within the meresnkyite field, but varying from a zone relatively close to the center of the triangle (~33 mol.% melonite, ~42 mol.% merenskyite, and ~21 mol.% moncheite) to the merenskyite apex but still containing some Pt (~3 mol.% melonite, ~84 mol.% merenskyite and ~15 mol.% moncheite) (Fig. 14). This extends the field for the merenskyite–melonite–moncheite solid solution system beyond that which was previously known. As merenskyite appears to have exsolved from BMS, its compositional variation along the fractionation trend reflects the variation that was in the sulfide melt. The sharp decrease of Ni content in the merenskyite towards eastern parts of the chonolith (Fig. 14) is expected as the sulfide liquid segregated from a more fractionated S-saturated magma containing lower base metals tenors, assuming that R- and N-factors are constant. This Ni depletion in the sulfide liquid segregated to the east is expressed by a lower pentlandite content (Table 3).

The massive sulfide ore sample 004-138.60 represents a different magma pulse as it is situated in the transition zone sequence (Fig. 6) rather than in the upper sequence. The composition of merenskyite in the transition zone plots in a distinct field that is clearly Pt and/or Ni depleted compared with merenskyite in massive sulfide ore in the upper sequence (Fig. 14). The magmatic system for the Limoeiro deposit is considered to result from the input of two major pulses of magma with similar compositions that have formed the upper and lower sequences (Mota-e-Silva et al. 2013). In view of the compositional differences in merenskyite, it is likely that the magma that formed the transition zone of the Limoeiro deposit was slightly depleted in Pt and/or Ni. If the transition zone was depleted in Pt, it is possible that sperrylite may have segregated from the silicate magma (Ballhaus and Sylvester 2000; McDonald 2008) or from the sulfide liquid (Dare et al.

Table 4 Compilation of several mineralized intrusion listing characteristics with potential to influence PGM size and Pd distribution between BMS and PGM

Intrusion (site)	Grades in deposit (g/t)	Depth of emplacement	Dimensions of intrusion (km)	Metamorphic facies	Median PGM size (largest grain) in μm^2	% of Pd in BMS	References
Limoeiro	0.2 Pt; 0.4 Pd	Upper crust	0.2×0.5×4	Upper amphibolite to granulite	6.4/88 (5000)	12–16	This study and Mota-e-Silva et al. (2013)
Noril'sk (Medvesky creek)	1.8 Pt; 7.3 Pd	Sub-volcanic	0.2×8×18	none	1.5	100	Barnes et al. (2008) and Naldrett (2004)
Buskveld (Merensky reef)	3.6 Pt; 1.8 Pd	Upper crust	7×280×450	none	620	30–60	Barnes et al. (2008) and Naldrett (2004)
Great Dyke (MSZ)	2.8 Pt; 2.1 Pd	Upper crust	3.5×7×400	none	4.5	30–60	Barnes et al. (2008) and Naldrett (2004)
Sudbury (Creighton deposit)	0.5 Pt; 0.6 Pd	Impact melt	2×30×60	Amphibolite	11 (3400)	40–90	Naldrett (2004), Dare et al. (2010a), Dare et al. (2010b), and Mukwakwami et al. (2012)
Penikat	1.7 Pt; 6.2 Pd	?	2×3×20	Greenschist	35	~50	Barnes et al. (2008)
Mirabela (Santa Rita)	0.1 Pt; 0.05 Pd	Lower crust	2×2×3	None	8 (690)	>50	Knight et al. (2011) and C.F. Ferreira Filho (personal communication, August 25, 2014)

2010a). Alternatively, the transition zone could be Ni depleted due to later-stage sulfide saturation after segregation of Ni-bearing silicate minerals (mainly olivine). The different timing of sulfide saturation between the upper sequence and the transition zone could be related to different levels of country rock assimilation. The upper sequence is generally thicker than the transition zone (Fig. 5), which responds to a more voluminous magma passing through that part of the conduit. A more voluminous magma is more likely to promote higher heat conduction into the substrate and achieve turbulent flow, which favors thermal erosion (Lesher et al. 2001).

The disseminated sulfide ore has a more diverse PGM assemblage with merenskyite accounting for 50 % of the PGM grains, accompanied by appreciable amounts of sperrylite, kotulskite, and moncheite (Fig. 7; ESM 3). The merenskyite grains located in the disseminated sulfide ore do not show the same compositional homogeneity within the same sample as identified in the massive sulfide ore (Table 1). Fine sulfide droplets are more able to be transported than coarse sulfide droplets or slugs of massive sulfide melt (Lesher and Groves 1986). The disseminated sulfide in the Limoeiro deposit is mainly formed by fine sulfide blebs between 50 and 400 μm in size (Mota-e-Silva et al. 2013), which were probably transported by magma fluxing through relatively long horizontal distances in the dynamic and sub-horizontal conduit system and finally they were trapped as inclusions in the settling silicates. Thus, the disseminated sulfide ore is composed of sulfide blebs crystallized in diverse parts of the magma conduit that have interacted with different magma compositions. This magmatic origin for disseminated sulfide heterogeneity relies on the fact that sulfide blebs in Limoeiro-disseminated sulfide still preserve their primary rounded geometry and mineralogy, which is composed of pyrrhotite (~70 vol.%), chalcopyrite (~15 vol.%), and pentlandite (15 vol.%) (Mota-e-Silva et al. 2013).

Arsenide is present in 8 % of the PGM in the Limoeiro deposit. In contrast to the bismuthotellurides, the arsenides are rarely found enclosed by the BMS but are more frequently found as euhedral to subhedral grains enclosed by silicate and oxide minerals or at the edge of BMS phases (Figs. 10 and 12). The phases that enclose the As-bearing sperrylite are primary magmatic orthopyroxene (Fig. 9a), magnetite crystals in sample 213-185.00 (Fig. 9b, f), and euhedral spinel, which is believed to represent a metamorphic transformation from chromite (Fig. 9e; Mota-e-Silva et al. 2013). Inclusions of Pt minerals in olivine and chromite were proposed to have formed by direct crystallization of PGM from the magma in the Merensky Reef (Ballhaus and Sylvester 2000). However, in the Limoeiro deposit, the sperrylite included in such phases is generally accompanied by a small chalcopyrite grain (Fig. 9a, f). Dare et al. (2010b) suggested that sperrylite and other sulfarsenides crystallized directly from the sulfide melt at temperatures above 1000 °C. Similar processes have also

been proposed for part of the arsenide assemblage in the Great Dyke of Zimbabwe (Coghill and Wilson 1993), for arsenide and sulfarsenide minerals in the Ni–Cu mineralizations at Dundonald Beach South, in Canada (Hanley 2007), formation of PGM in an As-rich magmatic sulfide system from the Talnotry diorite intrusion in Scotland (Power et al. 2004), and for the low sulfide, PGE-bearing rocks in the ultramafic complexes of Western Andriamena, Madagascar (McDonald 2008). McDonald (2008) suggested that the high As content in the initial sulfide melt promoted early crystallization of Pt, Ir, and Rh arsenide and sulfarsenide PGM, some of which segregated from the sulfide and were incorporated into growing olivine crystals. The textural associations at the Limoeiro deposit suggest the development of sperrylite predominantly by direct crystallization from sulfide melt. Sperrylite is the only arsenide identified in Limoeiro deposit, and As is below the LLD of 9 ppm in the BMS (Table 2). This suggests that all the As was used to form sperrylite, whereas Pt was abundant enough to remain in the sulfide liquid and enters into the merenskyite composition at the point in time that it exsolved from the BMS at <650 °C. The crystallization of sperrylite at high temperatures (>1000 °C) directly from sulfide melt has occasionally permitted sperrylite to form individual grains separated from sulfides during magma flow dynamics. The tiny sperrylite grains were kept in suspension within the magma as the flow dynamics can preferentially retain tiny grains compared with coarser sulfide liquid blebs that were partially accumulating at the bottom of the conduit to form the massive sulfide ore. This assumption explains why no sperrylite was identified in the massive sulfide ore (ESM 3). Alternatively, the massive sulfide layers represent MSS cumulates rather than the bulk sulfide liquid, and in this case, sperrylite may be included within the segregated intermediate solid solution (ISS). This possibility is supported by the observation that the massive sulfide ore of the Limoeiro deposit has high Ni/Cu ratios (between 3 and 5) compared with the disseminated sulfide (~0.75), suggesting that it represents MSS cumulates that segregated from Cu-rich residual sulfide liquid. Whether sperrylite is hidden within undiscovered Cu-rich offshoots or is indeed restricted to disseminated sulfide due to magma flow dynamics does not change the interpretation that the sperrylite crystallization conditions caused segregation from the sulfide blebs.

However, there are exceptions with a minority of the sperrylite grains present as anhedral rounded forms enclosed by BMS and in contact with an included silicate mineral (Fig. 9d), in a similar way to many of the merenskyite grains (Fig. 8a, b). These grains may represent a distinctly different generation of sperrylite and they might have been formed at a later-stage through exsolution from MSS.

The bulk Pt/Pd ratio is 0.33 in the western ore body (Retiro), whereas it is 0.38 in the eastern ore body (Piçarra; Fig. 16) indicating an overall increase in Pt relative to Pd to the east but, in contrast, the merenskyite becomes poorer in Pt to the east suggesting that the sulfide melt was relatively Pt depleted in the eastern part of the intrusion (Fig. 14). The conduit narrows from Retiro (west) to Piçarra (east) and we suggest that the mafic magma assimilated considerable amounts of As-rich country rock as it traveled eastwards along the conduit. As the country rocks are similar in Piçarra and Retiro, it is likely the Piçarra rocks record a higher degree of country rock contamination according to the presence of greater amounts of sulfides (Mota-e-Silva et al. 2013) and higher concentrations of Zn, Cd and Ag in the BMS (Table 2). Thus, it seems likely that: (i) during the magma flow from Retiro to Piçarra a significant amount of As was introduced from assimilation of the country rocks; (ii) the As was then incorporated into the sulfide melts that were present in the S-saturated magma flow; and (iii) the sulfide blebs crystallized early sperrylite due to As incompatibility in MSS (Hattori et al. 2002) and an affinity for Pt (Hutchinson and McDonald 2008). Almost all the As was expended to produce the crystallization of sperrylite, but this was not enough to consume all the Pt from the sulfide liquid. The remaining Pt was later incorporated into the merenskyite as the system cooled to temperatures of <650°C. The higher Pt/Pd ratio of Piçarra compared with Retiro is probably related to the greater abundance of sperrylite in the first. The magmatic processes described in the preceding sections and the metamorphic processes discussed in the sections that follow, are summarized in Fig. 18.

High-grade metamorphism

The Limoeiro Ni–Cu–(PGE) ore is strongly dominated by pyrrhotite with minor concentrations of chalcopyrite, pentlandite, and trace amounts of magnetite and pyrite (Mota-e-Silva et al. 2013). However, although it was metamorphosed to upper amphibolite to granulite facies conditions (700–850 °C), it has a typical magmatic sulfide ore deposit mineralogy, which would not melt under metamorphic facies below ultrahigh-temperature (UHT) metamorphism (Tomkins et al. 2007). However, during the cooling of the magmatic system, a residual liquid enriched in Cu, Pt, Pd, Au, Ag, As, Bi, Cd, Sb, Sn, Te, Pb, and Zn can segregate from the MSS (Li et al. 1992, 1996; Naldrett 2004; Helmy et al. 2010). The crystallization product of this residual sulfide liquid (ISS) is prone to remelt during amphibolite to granulite facies metamorphism (Tomkins et al. 2007). The Limoeiro massive sulfide layers may represent the solid phase (MSS) that has been separated from a residual sulfide liquid and therefore is unlikely to have melted during this metamorphism.

PGM stability indicates that merenskyite melts congruently at 740 °C (Medvedeva et al. 1961) and that it is unstable at temperatures above 500° to 540 °C (Hoffman and MacLean 1976). Sulfosalts or tellurides may start to melt at conditions ranging from lowest greenschist facies to amphibolite facies, well below conditions required for partial melting of common

silicate rocks. Thus, a complex PGE-bearing bismuthotelluride melt was probably generated in Limoeiro during the high-grade metamorphism. Because of the rarity of PGM, the proportion of melt produced by their decomposition is minuscule. This trace melt could sequestrate PGE during its fluxing through the volumetrically dominant sulfide (Tomkins et al. 2007). Arsenic, Pt, Pd, Au, Ag, Bi, Te, Sb, Pb are strongly incompatible with MSS (Holwell and McDonald 2010; Helmy et al. 2010) and have partition coefficients in the hundreds into sulfide, arsenide, or telluride liquids (Wood 2003; Hanley 2007; Helmy et al. 2007; Godel et al. 2012; Piña et al. 2013). However, the high-grade metamorphism was not hot enough to remelt sperrylite, which crystallized at temperatures >1000 °C in Limoeiro (Fig. 18).

Barnes et al. (2008) demonstrated that the slower cooling rate in a layered intrusion and possibly the presence of late-magmatic fluids can produce a greater degree of exsolution of the PGM than in the case of sub-volcanic sills. Thus, the length of time available for exsolution of the PGE from the MSS is proportional to the amount of PGE that are able to diffuse and exsolve as PGM instead of staying trapped within the structure of the BMS minerals. Neves and Alcantara (2010) using a combination of U/Pb and Ar/Ar isotopic methods identified that the metamorphic regional temperatures in the Limoeiro deposit region remained near the closing temperature of amphibole (~500 °C) for a long time (ca. 40 Ma) after the peak of metamorphism. The Limoeiro deposit has the lowest registered proportion of Pd housed within BMS (12-16 %) and one of the coarsest PGM assemblages despite its relatively low grades of Pt and Pd in a small and shallow intrusion (Table 4). The relatively long timeframe of the metamorphic conditions permitted the trace bismuthotelluride melt to efficiently interact with the BMS and scavenge most of PGE and their typical ligands to form discrete PGM phases after the metamorphic peak. It is likely that (i) the large grain size of merenskyite, (ii) high dominance of Pd in PGM rather than hosted by BMS, and (iii) compositional homogeneity among the dispersed merenskyite grains within any individual massive sulfide sample, are consequences of a metamorphic origin for the Limoeiro bismuthotellurides (Fig. 18). As an alternative hypothesis, the bismuthotellurides may have been absorbed in solid solution by the metamorphic MSS and later re-exsolved slowly after the high-grade metamorphism peak.

The upper amphibolite to granulite metamorphic recrystallization of the sulfide phases has not produced a distinct metamorphic mineralogy but one typical of magmatic ores. In contrast, other sulfide deposits worldwide, metamorphosed to lower grade sub-greenschist and greenshcist grades, display extensive alteration of the BMS assemblage forming magnetite-bearing pentlandite-rich sulfide aggregates, millerite, pyrite, and monoclinic pyrrhotite (Dillon-Leitch et al. 1986; Wang et al. 2008; Barnes et al. 2009; Smith et al. 2011; Djon and Barnes 2012). The reason why the Limoeiro ore has not modified from its primary compositions (i.e., no major S loss or gain, or Ni, etc.) is likely related to the absence of significant fluid infiltration during higher grade metamorphism. Under thermal metamorphism massive sulfide bodies recrystallize with the development of 120° triple-junction characteristic of equilibrated annealed textures (Craig 1983). The upper amphibolite to granulite facies metamorphism (700–850 °C) in Limoeiro was probably hot enough to drive BMS back into the MSS stability field. After the metamorphic peak, as system cooled down, re-crystallization of BMS generated a metamorphic honeycomb texture (Fig. 4b) with hexagons of pyrrhotite surrounded by chalcopyrite and pentlandite ribbons forming a 120° triple-junction fabric. As the high-grade metamorphism in the Limoeiro deposit was essentially thermal with a lack of coeval deformation, the sulfide did not move plastically. The merenskyite in Retiro's massive sulfide ores is commonly found in contact with spherical silicate minerals (Fig. 8a, b) composed of serpentine±hornblende±carbonate±chlorite. Abundant rounded silicate inclusions were identified in the massive sulfide of Tati and Selebi-Phikwe, in eastern Botswana (Fiorentini et al. 2012). Similar to the Limoeiro deposit, these intrusions are overprinted by granulite facies metamorphism.

Low-grade metamorphism, hydrothermalism and tectonism

Some PGM found in the Limoeiro deposit are affected by hydrothermal remobilization. This is shown by different textures including PGM within sulfide veinlets that crosscut the primary fabric (Fig. 13g, h), PGM within orthopyroxene (magmatic) and hornblende (metamorphic) cleavages (Fig. 13i, j), PGM enclosed by antigorite and apparently separated from the BMS (Fig. 13l), and PGM with irregular corroded contacts with the adjacent antigorite (Fig. 13e) or adjacent sulfide (Fig. 13f). The PGM that are associated with these late alteration textures are exclusively Pd-bearing minerals, essentially merenskyite (Fig. 12). Chloride and bisulfide are the most important ligands for Pd and Pt transport in hydrothermal fluid (Wood et al. 1989). Gammons et al. (1993) and Pan and Wood (1994) predict higher PdS solubility than PtS solubility as bisulfide complexes and suggest that Pd and Pt bisulfide complexes are important in Pd transport in hydrothermal fluids. Barnes and Liu (2012) found Pd to have higher solubility than Pt in hydrothermal systems in sulfide-rich environments. The removal of Pd by hydrothermal fluids can decouple Pd from Pt leaving behind rocks with relatively high Pt/Pd ratios (Fuchs and Rose 1974; Prichard et al. 2001). Coupling between deformation processes and rock permeability is a major factor influencing fluid migration in hydrothermal systems. The external part is the most deformed zone of the Limoeiro intrusion. Hydrothermal fluids have percolated

through this zone leaching bismuthotellurides, which are richer in Pd (abundant merenskyite) rather than Pt (rare moncheite). The extraction of metals produced a signature of a high Pt/Pd ratio in the amphibolite rocks in the most external part of intrusion (Fig. 17). Coevally, tectonic activity developed shear zones cross cutting the inner parts of the intrusion. These shear zones partly mobilized massive sulfide orebodies in plastic deformation allowing mobilization to produce distinctive "Durchbewegung" texture ores (Fig. 4c). The hydrothermal fluids deposited metals preferentially into the sheared massive sulfide orebodies, which have produced a distinctive assemblage consisting of hessite, Bi-rich merenskyite (Figs. 14 and 15) and chalcopyrite.

Conclusions

The principal conclusions of this study are as follows:

1. The Limoeiro intrusion parental magma was probably enriched in Te and Bi relative to other typical PGE ligands (As, Se, Sb, S), as shown by the extensive dominance of bismuthtellurides (~87 %) in the PGM assemblage.
2. Sperrylite crystallized early at high temperatures directly from sulfide blebs that were present in the Limoeiro magma conduit. The sperrylite is interpreted to have separated from the sulfide blebs and was captured as inclusions by high-temperature silicates and oxides.
3. Bi–Pt–Ni-bearing merenskyite is by far the dominant mineral phase in the Limoeiro PGM assemblage and is interpreted to have formed from crystallization from a PGE-bearing bismuthotelluride metamorphic melt or by exsolution from MSS during slow cooling. The merenskyite composition is controlled by the surrounding BMS composition.
4. The long timeframe of metamorphism permitted efficient diffusion of PGE through the BMS and the partition of Pd to the metamorphic bismuthotelluride melt. For this reason, Pd is by far more concentrated in PGM (84–88 %) than in BMS (12–16 %).
5. With increasing fractionation, the Pt/Pd ratio of the orebodies slightly increases, but the merenskyite becomes Pt and Ni poor. A decrease of Ni in the merenskyite composition reflects the composition of the sulfide liquid segregated from more fractionated magma to the east (Piçarra). The lower abundance of Pt in merenskyite is a consequence of Pt entering into sperrylite, which segregated in greater amounts from the sulfide liquid in that part of the intrusion during the magmatic stage.
6. Merenskyites in the transition zone have distinctly different compositions from those in the upper sequence. Merenskyite compositions vary with sulfide liquid composition, which depends on where the sulfide liquid segregated in terms of (i) magmatic stratigraphy and (ii) position in the fractionation trend from the west to the east of the complex.
7. Merenskyite grains in Limoeiro have different amounts of the melonite and moncheite end members in solid solution, showing enlarged field of solid solution for the merenskyite–melonite–moncheite system.
8. Low-grade metamorphism caused a heterogeneous removal of BMS, Pd, Te, and Bi from the outer parts of the chonolith. These fluids reprecipitated the metals as Bi-rich merenskyite and hessite assemblage in mobilized sulfide stringers in the inner parts of intrusion.

Acknowledgments We would like to thank the technical support from the Limoeiro Project team (headed by Rafael Freitas) for their assistance and cooperation. We are grateful to Jones Belther (Votorantim Metals' Minerals Exploration Division director) for permission to sample the Limoeiro deposit and publish the results. We are immensely glad with the very detailed corrections and suggestion of improvement carried out by the Associate Editor Mike Lesher, Editor-in-Chief Georges Beaudoin, Reviewer Belinda Godel, and an Anonymous Reviewer. This paper is part of first author's PhD thesis (Geosciences Institute, University of Brasilia), which was partly funded by CAPES Foundation, Ministry of Education of Brazil, fellowship (process BEX 3603/13-0).

Ethical Responsibilities of Authors This study was funded by CAPES Foundation, Ministry of Education of Brazil, fellowship (process BEX 3603/13-0). The authors declare that they have no conflict of interest.

References

Almeida FFM, Hasui Y, Brito Neves BB, Fuck RA (1981) Brazilian structural provinces: an introduction. Earth Sci Rev 17:1–29

Ames DE, Farrow CEG (2007) Metallogeny of the Sudbury mining camp. Mineral Deposits Division, Geological Association of Canada, Ontario, pp 329–350, Spec Pub 5

Ames DE, Davidson A, Wodicka N (2008) Geology of the giant Sudburypolymetallic mining camp, Ontario, Canada. Econ Geol 103:1057−1077

Ballhaus C, Sylvester P (2000) Noble metal enrichment processes in the Merensky Reef, Bushveld Complex. J Petrol 41:545–561

Barkov A, Laflamme G, Cabri LJ, Martin RF (2002) Platinum-group minerals from the Wellgreen Ni–Cu–PGE deposit, Yukon, Canada. Can Mineral 40:651–669

Barnes S-J, Lightfoot PC (2005) Formation of magmatic nickel sulfide ore deposits and processes affecting their copper and platinum group element contents. Econ Geol 100:179–213

Barnes SJ, Liu W (2012) Pt and Pd mobility in hydrothermal fluids: evidence from komatiites and from thermodynamic modelling. Ore Geol Rev 44:49–58

Barnes S-J, Couture JF, Sawyer EW, Bouchaib C (1993) Nickel-copper occurrences in the Belleterre-Angliers Belt of the Pontiac Subprovince and the use of Cu-Pd ratios in interpreting platinum-group element distributions. Econ Geol 88(6):1402–1418

Barnes S-J, Prichard HM, Cox RA, Fisher PC, Godel B (2008) The location of the chalcophile and siderophile elements in platinum-group element ore deposits (a textural, microbeam and whole rock geochemical study): implications for the formation of the deposits. Chem Geol 248:295–317

Barnes S-J, Wells MA, Verrall MR (2009) Effects of magmatic processes, serpentinization, and talc-carbonate alteration on sulfide mineralogy and ore textures in the Black Swan disseminated nickel sulfide deposit, Yilgarn Craton. Econ Geol 104(4):539–562

Beaty RD, Manuel OK (1973) Tellurium in rocks. Chem Geol 12(2):155–159

Brito Neves BB, Santos EJ, Van Schmus WR (2000) Tectonic history of the Borborema Province, Northeast Brazil. In: Cordani UG, Milani EJ, Thomaz Filho A, Campos DA (eds) Tectonic evolution of South America, 31st International Geological Congress, Rio de Janeiro, p 151–182

Cabri LJ (2002) The platinum-group minerals. In: Cabri LJ (ed) The geology, geochemistry, mineralogy and mineral beneficiation of platinum-group elements, Canadian Institute of Minning, Metallurgy and Petroleum, Spec Vol 54, pp 483–506

Cabri LJ, Laflamme G (1976) The mineralogy of the platinum group elements from some copper–nickel deposits of the Sudbury area, Ontario. Econ Geol 71:1159–1195

Coghill BM, Wilson AH (1993) Platinum-group minerals in the Selukwe Subchamber, Great Dyke, Zimbabwe: implications for PGE collection mechanisms and post-formational redistribution. Min Mag 57(389):613–634

Craig JR (1983) Metamorphic features in Appalachian massive sulphides. Min Mag 47(345):515–525

Dare SA, Barnes SJ, Prichard HM, Fisher PC (2010a) The timing and formation of platinum-group minerals from the Creighton Ni-Cu-platinum-group element sulfide deposit, Sudbury, Canada: early crystallization of PGE-rich sulfarsenides. Econ Geol 105(6):1071–1096

Dare SA, Barnes SJ, Prichard HM (2010b) The distribution of platinum group elements (PGE) and other chalcophile elements among sulfides from the Creighton Ni–Cu–PGE sulfide deposit, Sudbury, Canada, and the origin of palladium in pentlandite. Miner Deposita 45(8):765–793

Dillon-Leitch HCH, Watkinson DH, Coats CJA (1986) Distribution of platinum-group elements in the Donaldson West deposit, Cape Smith belt, Quebec. Econ Geol 81(5):1147–1158

Djon MLN, Barnes SJ (2012) Changes in sulfides and platinum-group minerals with the degree of alteration in the Roby, Twilight, and High Grade Zones of the Lac des Iles Complex, Ontario, Canada. Miner Deposita 47(8):875–896

Fiorentini ML, Bekker A, Rouxel O, Wing BA, Maier W, Rumble D (2012) Multiple sulfur and iron isotope composition of magmatic Ni-Cu-(PGE) sulfide mineralization from eastern Botswana. Econ Geol 107(1):105–116

Fuchs WA, Rose AW (1974) The geochemical behavior of platinum and palladium in the weathering cycle in the Stillwater Complex, Montana. Econ Geol 69(3):332–346

Gammons CH, Yu Y, Bloom MS (1993) Experimental investigation of the hydrothermal geochemistry of platinum and palladium: II. The solubility of PtS and PdS in aqueous sulfide solutions to 300 °C. Geochim Cosmochim Acta 57:2451–2467

Garuti G, Rinaldi R (1986) Mineralogy of melonitc-group and other tellurides from the Ivrea-Verbano Basic Complex, Western Italian Alps. Econ Geol 81:1213–1217

Godel B, Barnes S-J (2008) Platinum-group elements in sulfide minerals and the whole rocks of the J-M Reef (Stillwater Complex): implication for the formation of the reef. Chem Geol 248:272–294

Godel B, González-Álvarez I, Barnes SJ, Barnes SJ, Parker P, Day J (2012) Sulfides and sulfarsenides from the rosie nickel prospect, Duketon Greenstone Belt, Western Australia. Econ Geol 107(2):275–294

Hanley JJ (2007) The role of arsenic-rich melts and mineral phases in the development of high-grade Pt-Pd mineralization within komatiite-associated magmatic Ni-Cu sulfide horizons at Dundonald Beach South, Abitibi Subprovince, Ontario, Canada. Econ Geol 102(2):305–317

Harney DMW, Merkle RKW (1990) Pt-Pd minerals from the upper zone of the Eastern Bushveld Complex, South Africa. Can Mineral 28:619–628

Hattori KH, Arai S, Clarke DB (2002) Selenium, tellurium, arsenic and antimony contents of primary mantle sulfides. Can Mineral 40(2):637–650

Helmy HM, Ballhaus C, Berndt J, Bockrath C, Wohlgemuth-Ueberwasser C (2007) Formation of Pt, Pd and Ni tellurides: experiments in sulfide–telluride systems. Contrib Mineral Petrol 153(5):577–591

Helmy HM, Ballhaus C, Wohlgemuth-Ueberwasser C, Fonseca RO, Laurenz V (2010) Partitioning of Se, As, Sb, Te and Bi between monosulfide solid solution and sulfide melt—application to magmatic sulfide deposits. Geochim Cosmochim Acta 74(21):6174–6179

Helmy HM, Ballhaus C, Fonseca RO, Wirth R, Nagel T, Tredoux M (2013) Noble metal nanoclusters and nanoparticles precede mineral formation in magmatic sulphide melts. Nat Commun 4:2405

Hoffman EL, MacLean WH (1976) Phase relations of michenerite and merenskyite in the Pd-Bi-Te system. Econ Geol 71(7):1461–1468

Holwell DA, McDonald I (2010) A review of the behaviour of platinum group elements within natural magmatic sulfide ore systems. Platin Met Rev 54(1):26–36

Hudson DR (1986) Platinum-group minerals from the Kambalda nickel deposits, Western Australia. Econ Geol 81:1218–1225

Hutchinson D, McDonald I (2008) Laser ablation ICP-MS study of platinum-group elements in sulfides from the Platreef at Turfspruit, northern limb of the Bushveld Complex, South Africa. Miner Deposita 43(6):695–711

Kerr A (2001) The calculation and use of sulfide metal contents in the study of magmatic ore deposits: a methodological analysis. Explor Min Geol 10(4):289–301

Knight RD, Prichard HM, McDonald I, Ferreira CFF (2011) Platinum-group mineralogy of the Fazenda Mirabela intrusion, Brazil: the role of high temperature liquids and sulfur loss. Trans Inst Min Metall B 120(4):211–224

Kretz R (1983) Symbols for rock-forming minerals. Am Mineral 68:277–279

Lesher CM, Groves DI (1986) Controls on the formation of komatiite-associated nickel-copper sulfide deposits. In: Geology and metallogeny of copper deposits. Springer, Berlin, pp 43–62

Lesher CM, Burnham OM, Keays RR, Barnes SJ, Hulbert L (2001) Trace-element geochemistry and petrogenesis of barren and ore-associated komatiites. Can Mineral 39(2):673–696

Li C, Naldrett AJ, Coats CJA, Johannessen P (1992) Platinum, palladium, gold, copper-rich stringers at the Strathcona Mine, Sudbury; their enrichment by fractionation of a sulfide liquid. Econ Geol 87(6):1584–1598

Li C, Barnes SJ, Makovicky E, Rose-Hansen J, Makovicky M (1996) Partitioning of nickel, copper, iridium, rhenium, platinum, and palladium between monosulfide solid solution and sulfide liquid: effects of composition and temperature. Geochim Cosmochim Acta 60(7):1231–1238

Li C, Xu Z, de Waal SA, Ripley EM, Maier WD (2004) Compositional variations of olivine from the Jinchuan Ni–Cu sulfide deposit, western China: implications for ore genesis. Miner Deposita 39:159–172

Lightfoot PC, Farrow CEG (2002) Geology, geochemistry, and mineralogy of the Worthington offset dike: a genetic model for offset dike mineralization in the Sudbury Igneous Complex. Econ Geol 97:1419–1445

Lightfoot PC, Naldrett AJ, Gorbachev NS, Doherty W, Fedorenko VA (1990) Geochemistry of the Siberian Trap of the Noril'sk with implications for the relative contributions of crust and mantle to flood basalt magmatism. Contrib Mineral Petrol 104:631–644

Liu Y-N, Brenan J (2012) Experimental measurement of PGE and semi-metal partitioning during sulfide melt crystallization at controlled fO2-fS2 conditions. Chinese Academy of Sciences, 12th International Ni-Cu-(PGE) Symposium, China, Proceedings, pp 36–39

Lorand JP, Alard O, Luguet A, Keays RR (2003) Sulfur and selenium systematics of the subcontinental lithospheric mantle: inferences from the Massif Central xenolith suite (France). Geochim Cosmochim Acta 67(21):4137–4151

Makovicky E, Karup-Moller S, Makovicky M, Rose-Hansen J (1990) Experimental studies on the phase systems Fe-Ni-Pd-S and Fe-Pt-Pd-As-S applied to PGE deposits. Mineral Petrol 42:307–319

McDonald I (2008) Platinum-group element and sulfide mineralogy in ultramafic complexes at western Andriamena, Madagascar. Trans Inst Min Metall B 117(1):1–10

Medvedeva ZS, Klochko MA, Kuznetsov VG, Andreeva SN (1961) Structural diagram of the Pd-Te alloy system. Zh Neorg Khim 6: 1737–1739

Mota-e-Silva J, Ferreira Filho CF, Giustina MESD (2013) The Limoeiro deposit: Ni-Cu-PGE sulfide mineralization hosted within an Ultramafic tubular magma conduit in the Borborema Province, Northeastern Brazil. Econ Geol 108:1753–1771

Mukwakwami J, Lafrance B, Lesher CM (2012) Back-thrusting and overturning of the southern margin of the 1.85 Ga Sudbury Igneous Complex at the Garson mine, Sudbury, Ontario. Precambrian Res 196:81–105

Naldrett AJ (1981) Nickel sulphide deposits: classification, composition and genesis. Econ Geol 75:628–687

Naldrett AJ (2004) Magmatic sulfide deposits—geology, geochemistry and exploration. Springer, Berlin

Naldrett T, Kinnaird J, Wilson A, Chunnett G (2008) Concentration of PGE in the Earth's crust with special reference to the Bushveld Complex. Earth Sci Front 15(5):264–297

Neves SP, Alcantara VC (2010) Geochemistry of orthogneisses and metasedimentary rocks across a proposed terrane boundary in the Central Domain of Borborema Province, NE Brazil: geodynamic implications. J South Am Earth Sci 29(2):498–511

Pan P, Wood SA (1994) Solubility of Pt and Pd sulfides and Au metal in aqueous bisulfide solutions; II, results at 200 degrees C to 350 degrees C and saturated vapor pressure. Miner Deposita 29:373–390

Piña R, Gervilla F, Barnes SJ, Ortega L, Lunar R (2013) Partition coefficients of platinum group and chalcophile elements between arsenide and sulfide phases as determined in the Beni Bousera Cr-Ni mineralization (North Morocco). Econ Geol 108(5):935–951

Power MR, Pirrie D, Jedwab J, Stanley CJ (2004) Platinum-group element mineralization in an As-rich magmatic sulfide system, Talnotry, southwest Scotland. Mineral Mag 68(2):395–411

Prichard HM, Sá JHS, Fisher PC (2001) Platinum-group mineral assemblages and chromite composition in the altered and deformed Bacuri complex, Amapa, Northeastern Brazil. Can Mineral 39:377–396

Prichard HM, Knight RD, Fisher PC, McDonald I, Zhou MF, Wang CY (2013) Distribution of platinum-group elements in magmatic and altered ores in the Jinchuan intrusion, China: an example of selenium remobilization by postmagmatic fluids. Miner Deposita 48:767–786. doi:10.1007/s00126-013-0454-7

Santoliquido PM, Ehmann WD (1972) Bismuth in stony meteorites and standard rocks. Geochim Cosmochim Acta 36(8):897–902

Santos EJ, Van Schmus WR, Kozuch M, Brito Neves BB (2010) The Cariris Velhos tectonic event in northeast Brazil. J South Am Earth Sci 29:61–76

Seabrook CL, Prichard HM, Fisher PC (2004) Platinum-group minerals in the Raglan Ni–Cu–(PGE) sulfide deposit, Cape Smith, Quebec, Canada. Can Mineral 42(2):485–497

Sinyakova EF, Kosyakov VI (2007) Experimental modeling of zoning in copper-nickel sulfide ores. Dokl Earth Sci 417A(9):1380–1385

Smith JW, Holwell DA, McDonald I (2011) The mineralogy and petrology of platinum-group element-bearing sulfide mineralization within the Grasvally Norite–Pyroxenite–Anorthosite (GNPA) member, south of Mokopane, northern Bushveld Complex, South Africa. Trans Inst Min Metall B 120:158–174

Spear FS (1993) Metamorphic phase-equilibria and pressure—temperature—time paths. Mineral Society of America, Washington, D.C

Tomkins AG, Pattison DR, Frost BR (2007) On the initiation of metamorphic sulfide anatexis. J Petrol 48(3):511–535

Vokes FM (1969) A review of the metamorphism of sulphide deposits. Earth Sci Rev 5(2):99–143

Wang CY, Prichard HM, Zhou MF, Fisher PC (2008) Platinum-group minerals from the Jinbaoshan Pd–Pt deposit, SW China: evidence for magmatic origin and hydrothermal alteration. Miner Deposita 43(7):791–803

Whitney DL, Evans BW (2010) Abbreviations for names of rock-forming minerals. Am Mineral 95(1):185

Wilson AH, Murahwv CZ, Coghill B (2000) Stratigraphy, geochemistry and platinum group element mineralisation of the central zone of the Selukwe Subchamber of the Great Dyke, Zimbabwe. J Afr Earth Sci 30(4):633–653

Wood M (2003) Arsenic in igneous systems: an experimental investigation. BA Sc thesis, University of Toronto

Wood SA, Mountain BW, Fenlon BJ (1989) Thermodynamic constraints on the solubility of platinum and palladium in hydrothermal solutions; reassessment of hydroxide, bisulfide, and ammonia complexing. Econ Geol 84:2020–2028